Neuron

Development of top-down cortical propagations in youth

Highlights

- Cortical activity systematically propagates up and down a cortical hierarchy
- Bottom-up and top-down propagations are common in all participants across datasets
- Top-down propagations are more common during cognitive demands
- Top-down propagations become more prominent with development in youth

Authors

Adam Pines, Arielle S. Keller, Bart Larsen, ..., Leanne M. Williams, Damien A. Fair, Theodore D. Satterthwaite

Correspondence

satterth@pennmedicine.upenn.edu

In brief

Hierarchical processing requires activity propagating between higher and lower-order cortical areas. However, neuroimaging studies have chiefly quantified fluctuations within fixed regions over time rather than propagations over space. We used recent advances in neuroimaging and computer vision to demonstrate that top-down propagations become more prominent during task demands and over neurodevelopment.

Pines et al., 2023, Neuron *111*, 1–15
April 19, 2023
https://doi.org/10.1016/j.neuron.2023.01.014

CellPress

Neuron

CellPress

Article

Development of top-down cortical propagations in youth

Adam Pines,[1,2,3] Arielle S. Keller,[2,3] Bart Larsen,[2,3] Maxwell Bertolero,[2,3] Arian Ashourvan,[4] Dani S. Bassett,[3,5,6,7,8,9,10] Matthew Cieslak,[2,3] Sydney Covitz,[2,3] Yong Fan,[11] Eric Feczko,[12] Audrey Houghton,[12] Amanda R. Rueter,[12] Manish Saggar,[1] Golia Shafiei,[2,3] Tinashe M. Tapera,[2,3] Jacob Vogel,[2,3] Sarah M. Weinstein,[7] Russell T. Shinohara,[7] Leanne M. Williams,[1] Damien A. Fair,[12] and Theodore D. Satterthwaite[2,3,13,*]

[1]Department of Psychiatry and Behavioral Sciences, Stanford University, Stanford, CA 94304, USA
[2]The Penn Lifespan Informatics and Neuroimaging Center, University of Pennsylvania, Philadelphia, PA 19104, USA
[3]Department of Psychiatry, Neurodevelopment & Psychosis Section, University of Pennsylvania, Philadelphia, PA, USA
[4]Department of Psychology, The University of Kansas, Lawrence, KS 66045, USA
[5]Departments of Bioengineering, University of Pennsylvania, Philadelphia, PA 19104, USA
[6]Department of Neurology, University of Pennsylvania, Philadelphia, PA 19104, USA
[7]Department of Biostatistics, Epidemiology, and Informatics, University of Pennsylvania, Philadelphia, PA 19104, USA
[8]Department of Electrical & Systems Engineering, University of Pennsylvania, Philadelphia, PA 19104, USA
[9]Department of Physics & Astronomy, The University of Pennsylvania, Philadelphia, PA 19104, USA
[10]Santa Fe Institute, Santa Fe, NM 87051, USA
[11]Department of Radiology, The University of Pennsylvania, Philadelphia, PA 19104, USA
[12]Masonic Institute for the Developing Brain, Institute of Child Development, College of Education and Human Development, Department of Pediatrics, Medical School, University of Minnesota, Minneapolis, MN 55414, USA
[13]Lead contact
*Correspondence: sattertt@pennmedicine.upenn.edu
https://doi.org/10.1016/j.neuron.2023.01.014

SUMMARY

Hierarchical processing requires activity propagating between higher- and lower-order cortical areas. However, functional neuroimaging studies have chiefly quantified fluctuations within regions over time rather than propagations occurring over space. Here, we leverage advances in neuroimaging and computer vision to track cortical activity propagations in a large sample of youth (n = 388). We delineate cortical propagations that systematically ascend and descend a cortical hierarchy in all individuals in our developmental cohort, as well as in an independent dataset of densely sampled adults. Further, we demonstrate that top-down, descending hierarchical propagations become more prevalent with greater demands for cognitive control as well as with development in youth. These findings emphasize that hierarchical processing is reflected in the directionality of propagating cortical activity and suggest top-down propagations as a potential mechanism of neurocognitive maturation in youth.

INTRODUCTION

The hierarchical organization of the cortex provides a scaffold for bottom-up sensory integration and top-down control.[3–6] In humans, this hierarchical cortical organization is critical for cognitive control and executive function.[7–9] However, recent evidence suggests that this cortex-wide hierarchical organization is not established at birth but is instead a product of protracted development.[10–12] Critically, the establishment of this cortical hierarchy is contemporaneous with both the development of top-down executive function[12,13] and the onset of psychiatric disorders.[14,15] Understanding this neurodevelopmental window is crucial, as deficits in top-down control are associated with transdiagnostic psychopathology,[16] reduced quality of life,[17] and mortality in youth.[18] Although functional magnetic resonance imaging (fMRI) allows for noninvasive imaging of neurocognitive development, it has remained challenging to identify the precise spatiotemporal patterns of activity that support the development of top-down processing.

Notably, top-down hierarchical processing necessarily involves activity propagating through space from higher- to lower-order areas. However, most fMRI studies of hierarchical processing have quantified activity fluctuations in fixed regions over time rather than accounting for activity propagations over space. Recently, three studies have used a combination of fMRI in humans and intracranial recordings in macaques to show that slow but widespread activity systematically propagates up a putative cortex-wide functional hierarchy (FH)[19–21] known as the principal gradient.[22] The observation of systemic propagations up the principal gradient provides a particularly compelling account of hierarchical activity for two reasons. First, the principal gradient itself reconciles several prominent theories

Please cite this article in press as: Pines et al., Development of top-down cortical propagations in youth, Neuron (2023), https://doi.org/10.1016/j.neuron.2023.01.014

of hierarchical cortical organization.[22–26] Second, the observation of "bottom-up" propagations ascending the principal gradient aligns with proposed mechanisms of bottom-up hierarchical processing.[10,23,25,26] Further, two recent studies documented top-down propagations, where alertness[19] and arousal[27] were associated with the movement of activity from higher- to lower-order cortical regions. Together, these studies suggest that the direction of cortical activity over space (bottom-up or top-down) may be linked to hierarchical processing.

Despite these recent advances, important gaps remain. First, prior approaches to quantifying propagations have required summarizing activity across the entire brain in order to determine hierarchical directionality. Although these approaches can reveal whole-cortex hierarchical patterns of activity propagations, work in animal models suggests that cortical propagations may be predominantly localized phenomena. In contrast to the large white matter bundles typically posited as the structural basis for functional network connectivity,[28,29] cortical surface propagations utilize relatively shorter, horizontal projections.[30–38] Second, developing noninvasive approaches that can capture local spatial directionality of activity propagations remains an important unmet need, as prior work has suggested that propagation directionality may be a central feature of stimulus encoding and task execution.[30–32,39–41] Third, in addition to summarizing activity over the whole brain, existing fMRI approaches to delineating the procession of activity over space have typically required collapsing activity over many individuals. As a result, prior studies have not evaluated individual differences in cortical propagations at the local scale at which they are thought to occur. Individual differences are likely to be particularly informative for studies of brain development in youth, as top-down cognitive control improves dramatically in childhood and adolescence. However, it remains unknown whether top-down propagations become more prominent with development in youth.

Here, we fill this critical gap by applying a method that has been widely used in computer vision—optical flow—to quantify the direction of activity propagations across the cortex in a large sample of youth. In contrast to other measures of fMRI signal fluctuations, optical flow enables the quantification of the directional trajectory of activity over space on the surface of the cortex. We applied optical flow to a large developmental dataset that included both high-quality resting-state and task-fMRI data[1] and evaluated whether the direction of propagating signals aligned with the FH established by the principal gradient. We hypothesized that our approach would reveal both intra- and inter-individual differences in bottom-up and top-down propagations. Specifically, we predicted that top-down propagations would become more prominent within individuals in response to a task that required cognitive control. Furthermore, we predicted that a comparison between individuals would reveal an increased prevalence of top-down hierarchical propagations with age in youth.

RESULTS

We capitalized upon advances in computer vision and a large sample of youth studied using fMRI at a high temporal resolution to identify hierarchical propagations of cortical activity and delineate how they evolve with age. Specifically, our sample included n = 388 participants ages 8–22 years old (204 female participants) from the Human Connectome-Development (HCP-D) project who had a large quantity (mean number of TRs per participant remaining after quality control = 1,255.7) of low-motion fMRI data acquired at rest. The spherical registration of these data enabled us to leverage spherical optical flow[42,43] to identify propagations of activity occurring across the cortical surface. Below, we first introduce the analytic framework for the application of optical flow and demonstrate that this technique can accurately identify activity propagations in simulated data with realistic noise properties where the ground truth is known. Using real data from HCP-D, we subsequently show that hierarchical cortical propagations can be found in every individual participant in this large dataset—we replicate this finding in a sample of densely sampled adults. Next, we establish that tasks that require cognitive control are associated with more top-down cortical propagations and delineate increases in the prevalence of top-down propagations with age in youth. Finally, we present analyses that emphasize that these effects cannot be explained by developmental changes in functional connectivity and are robust to alternative definitions of the cortical hierarchy.

Measuring activity propagations across the cortical hierarchy with optical flow

Optical flow is a widely used computer vision technique[44,45] that measures intensity differences between successive pairs of images and estimates how intensity values in the image move from one frame to the next. Ultimately, this procedure yields a vector field between each frame—these vectors describe the direction of movement of intensity values between frames at each location in the image. We applied this approach to individual fMRI time series, where image intensity differences reflect differences in the blood-oxygen-level-dependent (BOLD) signal. As the BOLD signal reflects local field potentials,[19,20,46–50] the resultant vector fields described the direction of activity propagation between pairs of sequential fMRI volumes (Figure 1A). To evaluate whether fMRI activity propagates hierarchically, we compared the vector field derived from optical flow with a widely used map of the cortical FH[22] (Figure S1). We evaluated the spatial gradient (∇) of the FH to derive a vector field that describes the direction of ascent up the hierarchy at each point on the cortex—we refer to this map of vectors as ∇FH. The directions described by ∇FH served as a reference that allowed us to describe the observed directional movement of activity quantified by optical flow as ascent or descent along the FH. Specifically, we calculated the difference in the angle (in degrees) of the direction of activity estimated by optical flow compared with the direction of hierarchical ascent defined by ∇FH (Figure 1C). This comparison was repeated for each pair of time points, generating a time series of angles at each location that reflected the degree to which the estimated direction of activity propagations aligned with a hierarchical ascent over time (Figure 1D). In this framework, alignment with the angle of hierarchical ascent (0° from ∇FH) indicated a bottom-up hierarchical propagation, whereas flow in the opposite direction (180° from ∇FH) indicated a top-down hierarchical propagation (Figures 1E, S2, and S3).

Please cite this article in press as: Pines et al., Development of top-down cortical propagations in youth, Neuron (2023), https://doi.org/10.1016/j.neuron.2023.01.014

CellPress

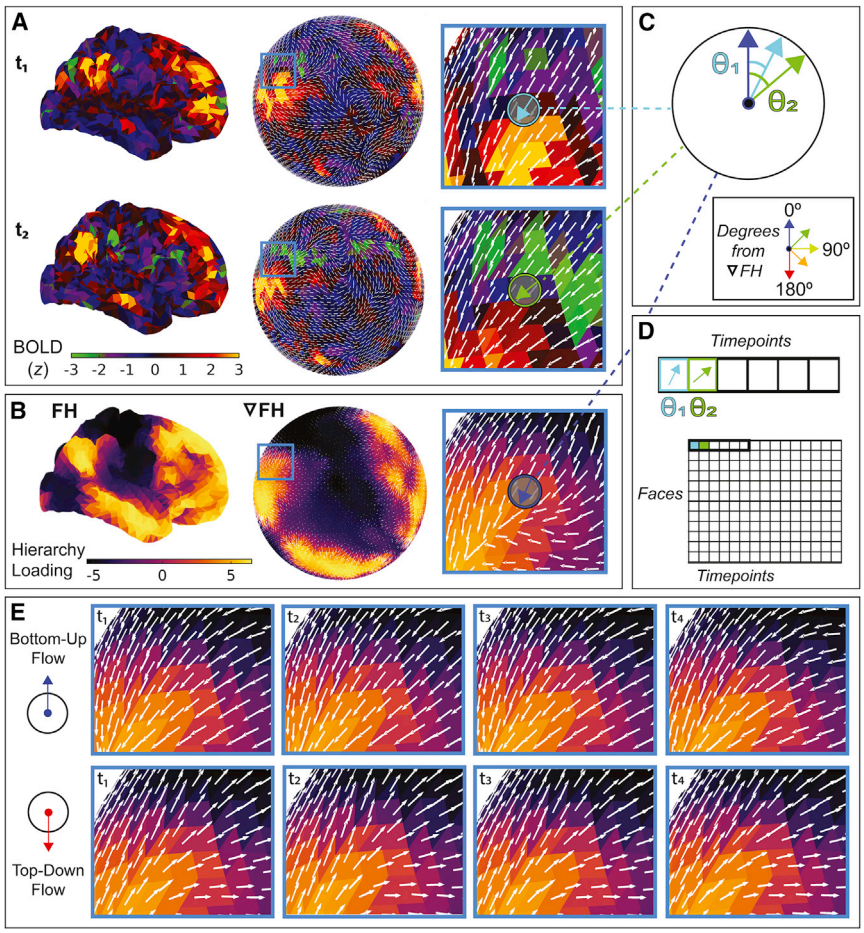

Figure 1. Measurement of hierarchical cortical propagations using optical flow

(A) To estimate the spatial directionality of activity across the cortex, all fMR images are projected to the *fsaverage4* spherical surface. Specifically, for each pair of sequential images, we use optical flow to estimate the directions of signal propagations between each pair of successive images for each face on the cortical mesh.

(B) To estimate the direction of hierarchical ascent, the gradient vector field of a widely used map of the functional cortical hierarchy[22] was extracted along the cortical surface (∇FH). This procedure yields vectors across the entire cortex, with each vector describing the most immediate direction of hierarchical ascent for any given face on the mesh.

(C) To quantify directional distributions, each optical flow direction was assessed relative to the ∇FH (direction of hierarchical ascent) over all sequential image pairs.

(D) This procedure was repeated for each face on the cortical mesh to yield a matrix of activity directions relative to ∇FH over time for each participant.

(E) Example bottom-up and top-down propagations: vectors were extracted from pairs of sequential BOLD images (white arrows) and overlaid onto the group-level FH (yellow-black shading). FH, functional hierarchy.

Simulations reveal that optical flow captures cortical propagations

To ensure that our analytic framework was capable of accurately detecting cortical propagations in fMRI data, we generated simulations of cortical propagations where the ground truth was known. Simulated data were matched to the spectral content and noise properties of real fMRI data[19–21,51] (see STAR Methods). Specifically, we generated a synthetic wave of activation that propagated in the posterior-to-anterior direction across the cortical surface (Figure 2A). To create a corresponding reference vector field (equivalent to ∇FH), we also created a scalar map that quantified the posterior-to-anterior position of each face on the surface of the cortex (Figure 2B) and calculated the gradient (∇) of this scalar map (∇PA, Figures 2C and 2D). Measurement of the vector fields obtained from the simulated data relative to ∇PA revealed a prominent alignment of the directions recovered by optical flow with the known ground truth (92.3% of directions within 90 degrees of ∇PA, 8.49 SD from null directions, $p < 0.001$; Figure 2E), and tighter alignment was limited by the realistic noise properties of the simulated data. These results from simulated data suggest that optical flow can accurately capture the directionality of cortical activity propagations.

Optical flow reveals hierarchical propagations of cortical activity

Having verified that optical flow can accurately characterize the directionality of cortical propagations in simulated data, we next applied this approach to the real data from HCP-D. We expected to find both bottom-up propagations that aligned with the FH (angular distances close to 0° compared with the ∇FH) as well as top-down propagations that flowed in the opposite direction (angular distances 180° from ∇FH). As hypothesized, we found a predominance of both bottom-up and top-down hierarchical propagations, which formed a bimodal distribution. These bimodal distributions were evident at both the group (Figure 3A) and participant level (Figure 3B). To test whether propagations were enriched for bottom-up and top-down directionality, we quantified the presence of a bimodal distribution in each participant's data using the dip statistic. We then compared this value with a null distribution generated using a conservative spin-based permutation test that persevered the spatial covariance structure of the data. This procedure revealed that the angular distributions of propagations were bimodal in every single participant in the HCP-D sample, far beyond what could be expected by chance (real data median SD from null distribution = 13.6 SD; $p < 0.001$ for all participants in the sample; Figure 3C). To further confirm that optical flow captured continuous propagations rather than differences between discrete activation patterns, we shuffled the temporal ordering of fMRI volumes for each participant. These temporal permutation tests confirmed that optical flow captured specific sequences of activity that were

Please cite this article in press as: Pines et al., Development of top-down cortical propagations in youth, Neuron (2023), https://doi.org/10.1016/j.neuron.2023.01.014

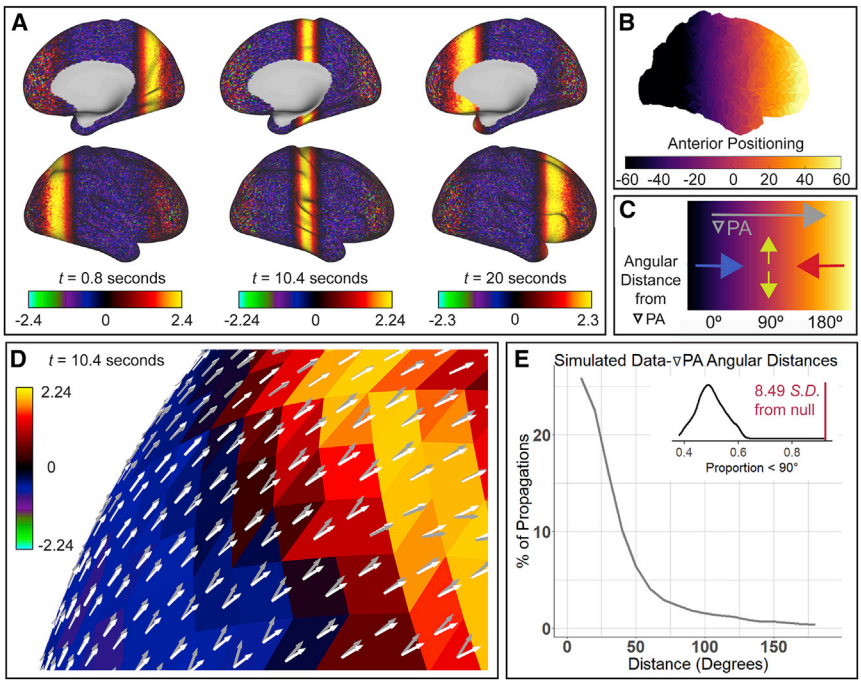

Figure 2. Optical flow accurately recovers directional propagations in simulated fMRI data

(A) We simulated a wave that travels from the posterior pole to the anterior pole over ≈ 20 s. Realistic human BOLD spectral content was enforced in accordance with Laumann et al.[51]

(B) To create a reference direction equivalent to ∇FH, we use a scalar map of the posterior-to-anterior (PA) positioning of each point on the cortex.

(C) We calculated the gradient of this scalar posterior-anterior map (∇PA) over the cortical surface to serve as a directional reference for the cortex to calculate simulated propagation directionality.

(D) Example directional estimations of optical flow on the simulated wave. White arrows depict activity directionality as estimated by optical flow, and gray vectors depict ∇PA.

(E) Across cortical areas and time points, angular distances between the directions estimated by optical flow aligned with the expected ∇PA reference direction. Inset (top right) depicts the proportion of optical flow vectors within 90° of ∇PA relative to 1,000 null-reference direction distributions (Observed = 0.923, 8.49 SD from null directions).

not present in temporally shuffled data (real data median SD from null distribution = 18.8 SD; $p < 0.01$ for 93% of participants in the sample; Figure 3D). These data suggest that bottom-up and top-down propagations are common and robust features of cortical activity.

Hierarchical propagations are also found in a dataset of densely sampled adults

As a next step, we sought to replicate our findings using an independent dataset of adults. To this end, we applied the same procedures to the densely sampled participants of the Midnight Scan Club (MSC) dataset. We found that hierarchical propagations were also present in all 10 MSC participants (Figure 4). This generalization is notable given the different age ranges, scanning hardware, and temporal qualities of the data (which included a nearly 3-fold decrease in temporal resolution in MSC compared with HCP-D). These results suggest that hierarchical activity propagations are a generalizable feature of cortico-functional activity in both youth and adults.

Top-down cortical propagations increase during a task that requires cognitive control

Having described the presence of hierarchical activity propagations at rest, we next sought to determine whether they were modulated by the performance of a demanding cognitive task. Specifically, we hypothesized that the proportion of top-down cortical propagations relative to bottom-up propagations would increase when participants performed a task requiring cognitive control. To define the spatial distribution of bottom-up and top-down propagations, we quantified the percentage of propagations that could be characterized as bottom-up (< 90° from ∇FH) or top-down (> 90° from ∇FH) for each location on the cortex (Figure 5A). Notably, although all regions exhibited a mix of both bottom-up and top-down propagations, top-down propagations were enriched in regions such as the dorsolateral prefrontal cortex. At the participant level, the percentage of top-down optical flow vectors was highly correlated with our statistical summary measure of bimodality (i.e., dip statistic, $r = 0.70$, $p < 2.2 \times 10^{-16}$; Figure 5B). Examining the percentage of top-down propagations allowed us to directly test whether top-down propagations became more common when participants performed a cognitive control task.

We compared propagations observed during rest with those present during a modified Go/NoGo task, where top-down control is required to suppress reflexive button-pressing[1] (Figure 6A). Mass univariate analyses revealed more top-down propagations during task than rest ($n = 281$, $t_{face} = 2.37–13.97$, $p_{fdr} < 0.05$). Although these effects were distributed across the cortex, increases in top-down propagations were particularly prominent in regions within the dorsal and ventral attention systems. Increases were maximal in the left upper-extremity subdivision of the motor cortex, likely reflecting participants using their right hand to perform the task[1] (Figure 6B). These results suggest that task demands evoke increased prominence of top-down propagations within individuals.

Top-down cortical propagations increase over the development

Given that we observed an increase in top-down cortical propagations during a cognitive control task and that cognitive control abilities improve with age, we next evaluated whether top-down propagations became more prevalent with age in our sample of youth. Developmental effects were modeled with penalized splines that capture both linear and nonlinear effects—sex,

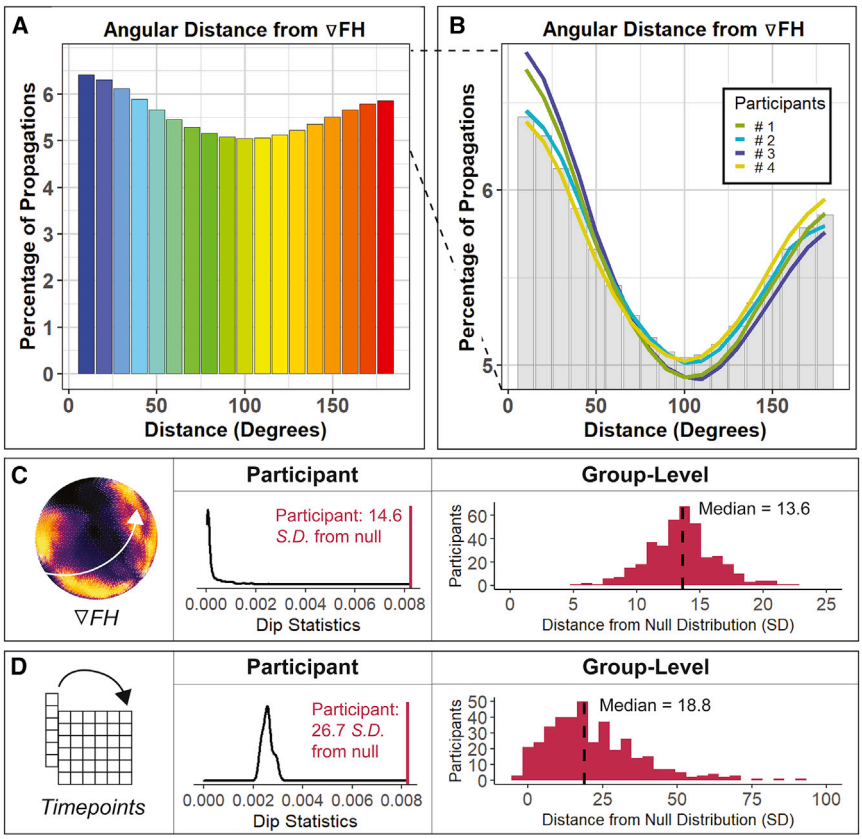

Figure 3. Hierarchical propagation of cortical activity

(A) Across the entire sample, we found a bimodal distribution of angular distances between the ∇FH and vectors of directional activity estimated by optical flow (4.4 billion optical flow directions over all participants, locations, and time points).

(B) Directional distributions formed a bimodal distribution enriched for hierarchical ascent (0°) and descent (180°) within individual participants. The percentage axis is rescaled from (A) for detail, with the equivalent y axis range demarcated across panels with dashed lines. The dip statistic was used to quantify the bimodality of each participant's distribution of directional activity vectors and used in subsequent statistical testing.

(C) Spatial null models spun the reference directions provided from ∇FH, preserving the spatial covariance structure of the original map (left). Spatial null models were computed within participants (middle; participant #1 from B) by comparing the dip statistic obtained from permuted reference directions (black distribution) and the dip statistic from the real data (red line). Whereas 1.64 standard deviations from the mean is a common statistical threshold for significance, we found that the distribution of dip statistics from all the participants in the sample was approximately 13.6 standard deviations from the null distribution (right).

(D) Temporal null models shuffled the order of retained fMRI volumes in time, preserving complex spatial patterns found within individual images (left). Temporal null models were computed within participants (middle; participant #1 from B) by comparing the dip statistic obtained from permuted fMRI volume ordering (black distribution) and the dip statistic observed in real data (red line). Observed dip statistics were a median of 18.8 standard deviations from the null distribution (right). Note: 5 participants with positive outlier values are omitted for clarity (SDs = 166.7, 189.3, 258.9, 369.7, and 747.9).

number of frames available, and in-scanner head motion were included as model covariates. We found that older age was associated with widespread increases in the proportion of top-down propagations across the cortex (Δ Adjusted R^2 = 0.01–0.19, $p_{fdr} < 0.05$, Figure 7A). These effects were particularly prominent in the anterior cingulate cortex, dorsal and ventral visual streams, and the medial and lateral premotor pathways. Age associations extended continuously between the canonical medial premotor pathway and inferior-medial prefrontal cortex, suggesting an overlap in the maturation of regions in the default-mode network and maturation of the internally driven medial premotor pathway. This increased prevalence of top-down propagations with age was quite evident even when measurements were averaged across the entire cortex (Δ Adjusted R^2 = 0.14, p = 1.7 × 10^{-14}, Figure 7B; Table S1).

Notably, the above analyses rely on a binarization of propagations into bottom-up or top-down. Next, we investigated how development is associated with shifts in the full distribution of directional propagations. To do so, we calculated the difference in the average angular distribution of propagations for the youngest (n = 127, mean age = 11.49, SD = 1.70 years) and oldest (n = 132, mean age = 19.76, SD = 1.39 years) tertiles of the data (Figure 7C). We then evaluated the significance of this difference in distributions by comparing the true difference to a null distribution created from random tertile splits (Figure 7C, gray band). We found that the angular distributions shifted monotonically toward top-down propagations with age: maximally top-down propagations increased with age the most, whereas maximally bottom-up propagations showed the largest declines with age. Together, these results suggest that top-down cortical propagations are a prominent feature of functional brain development.

Hierarchical propagations are robust to analytic parameter choices and choice of the cortical hierarchy

Next, we conducted a series of sensitivity analyses to bolster confidence in our results. First, we sought to further confirm that the detection of hierarchical cortical propagations was not contingent upon a specific set of spatial regularization parameters used by the optical flow algorithm. To do so, we repeated our spatial permutation tests (as in Figure 3C) for all participants while applying a wide range of spatial regularization parameters. Across the HCP-D sample, we found that the angular distributions of propagations were specifically aligned with the FH for every parameter choice that we evaluated (Figure S4). These results suggest that the detection of bottom-up and top-down propagations is not dependent on specific analytic parameter choices.

Please cite this article in press as: Pines et al., Development of top-down cortical propagations in youth, Neuron (2023), https://doi.org/10.1016/j.neuron.2023.01.014

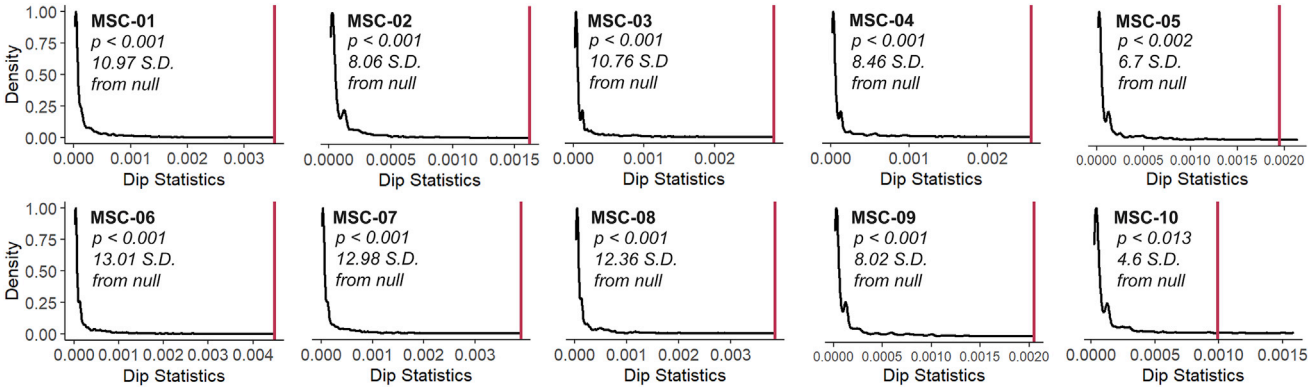

Figure 4. Cortical activity propagates up and down the cortical hierarchy in an independent sample

Spatial null permutation testing reveals the presence of bimodal cortical propagations for all midnight scan club participants (black, spin-test permutations; red, true dip statistic).

Next, we sought to determine whether our findings would remain consistent if an alternate account of the cortical hierarchy was used. Although the FH is among the most widely used, a structural hierarchy (SH) defined by the presence of intracortical myelin is also broadly accepted. Prior work has demonstrated that this SH defined by cortical myelin content aligns with hierarchical measures of tract tracing and gene expression.[52,53] We used a myelin map derived from HCP-D that corrected for transmit field bias[54] and repeated our main analyses with ∇SH instead of ∇FH (STAR Methods; Figure 8A). First, we evaluated whether cortical propagations traverse up and down the cortical hierarchy using the same conservative spatial permutation procedure. Observed dip statistics remained far (median = 8.6 standard deviations away) from our spatial null distribution, indicating that cortical propagations traverse up and down the SH far more frequently than expected by chance (Figure 8B). Next, we compared propagations present during the cognitive control task with those present at rest using the SH as the reference. The spatial distribution of results was highly similar to that observed when the FH was used as a reference (Figure 8C). Similarly, when the SH was used as a reference, we found that age was associated with greater prevalence in top-down propagations (Δ Adjusted R^2 = 0.10, p = 2.8 × 10^{-10}; Figure 8D). Finally, as prior, we calculated the difference in the average angular distribution of propagations for the youngest and oldest tertiles of the data. When using ∇SH instead of ∇FH, we also found that the angular distributions consistently shifted toward fewer bottom-up and greater top-down propagations with age (Figure S5). Together, these results suggest that the existence of hierarchical propagations, the presence of task-evoked shifts in propagations, and observed associations with development are robust to definitions of the cortical hierarchy.

The development of top-down activity propagations is distinct from the development of functional connectivity

Having demonstrated the presence of age-related increases in top-down propagations, we next conducted specificity analyses to evaluate if the observed development of top-down propagations were dissociable from previous descriptions regarding the development of functional connectivity. Notably, the spatial distribution of the principal gradient is collinear with the distribution of functional networks,[22] and the age associations we report occur over the same age range as developmental functional network segregation.[12,55] In particular, default

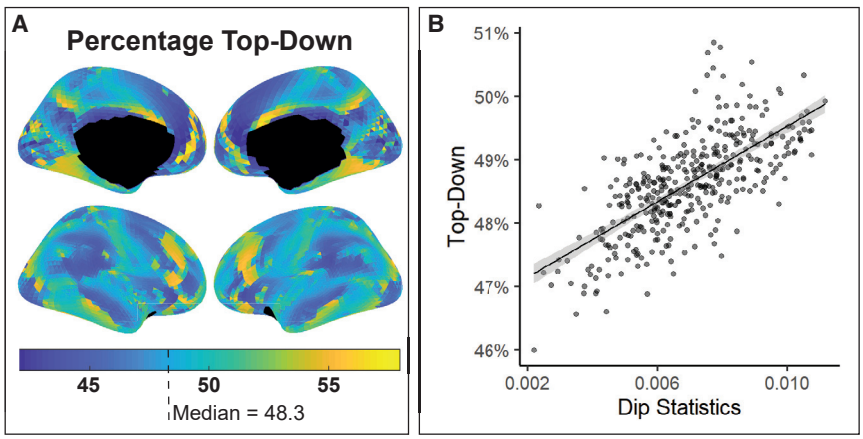

Figure 5. Top-down propagations differ across the cortex and individuals

(A) All faces exhibited a mix of both bottom-up (<90° from ∇FH) and top-down (>90°) propagations, but certain regions were enriched for bottom-up propagations or top-down propagations. For example, bottom-up propagations were more common in the medial prefrontal cortex, whereas top-down propagations were more common in the dorsolateral prefrontal cortex.

(B) Across participants, top-down propagations were strongly associated with a bimodal distribution of directional propagations quantified by the dip statistic (r = 0.70, p < 2.2 × 10^{-16}). The 95% confidence interval of this linear relationship is indicated by the shaded area.

Please cite this article in press as: Pines et al., Development of top-down cortical propagations in youth, Neuron (2023), https://doi.org/10.1016/j.neuron.2023.01.014

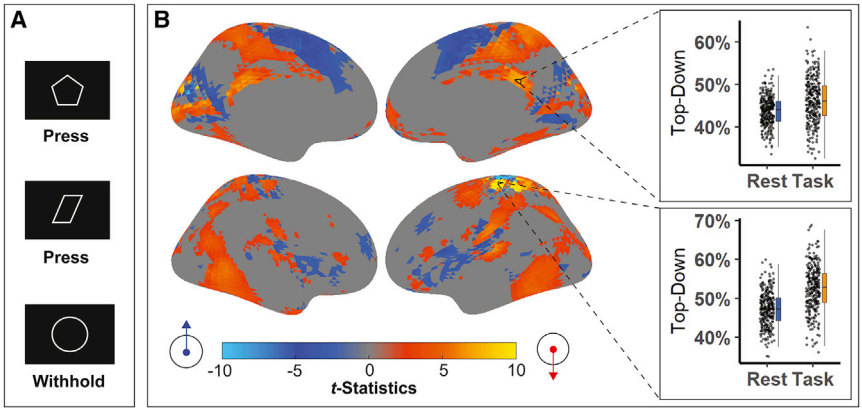

Figure 6. A cognitive control task is associated with an increase in top-down propagations

(A) Schematic for Go/NoGo task where participants are asked to immediately press a button in response to certain shapes and to withhold their response when presented with others.

(B) Map of significant differences in top-down propagations between task and rest ($P_{FDR} < 0.05$). Blue areas indicate faces where bottom-up propagations are more common during task demands (30% of statistically significant faces) and orange areas indicate faces where top-down propagations are enriched during task demands (70% of statistically significant faces). Insets (right) depict example task-rest differences at two cortical faces.

mode network segregation has been among the most consistently reported aspects of adolescent functional connectivity maturation.[12,55–62] Consequently, we sought to ensure that the development of hierarchical propagations was not attributable to differences in default mode segregation with age. Specifically, we quantified default-mode network segregation in all participants (STAR Methods) and repeated our developmental analyses of top-down propagations while covarying for individual differences in default-mode network segregation. We found that the association between top-down propagations and age

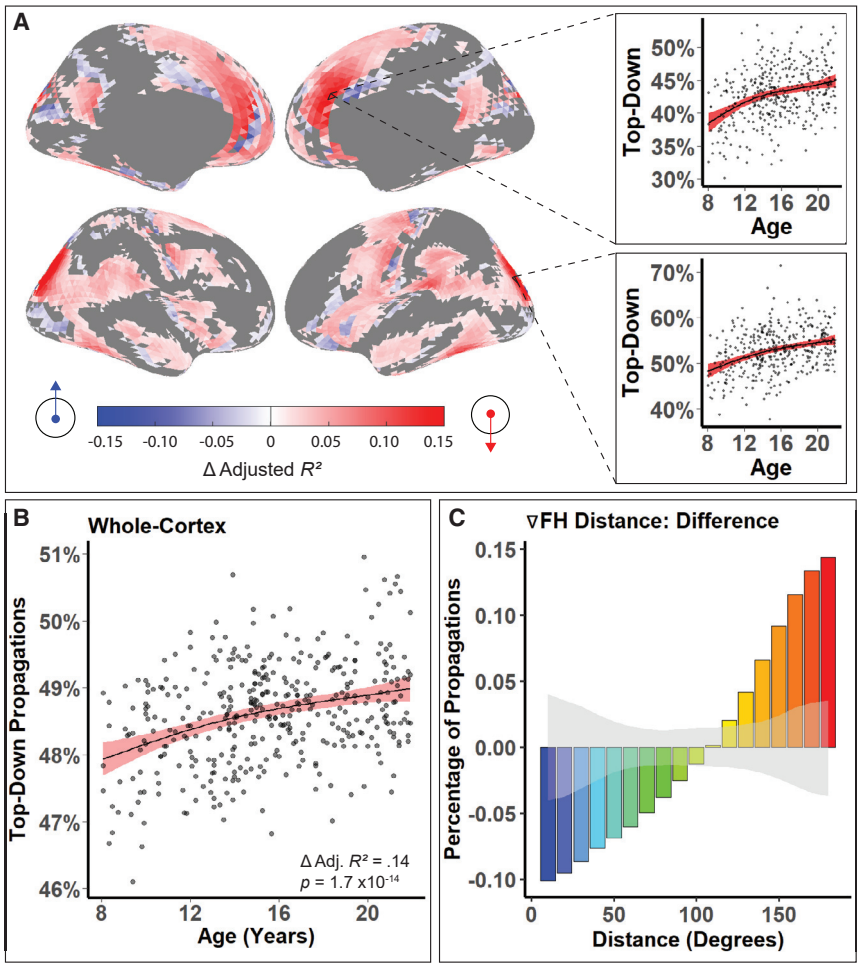

Figure 7. The prevalence of top-down propagations increases with age

(A) Top-down propagations become more prominent with age in youth ($p_{FDR} < 0.05$, more top-down with age in red).

(B) When averaged across the cortex, top-down propagations increase with age (smooth term effective degrees of freedom = 1.89).

(C) Whole-cortex directional distributions mature such that after adolescence, a greater percentage of propagations are top-down. This difference extends above and beyond the 95th percentile of distribution differences observed in 1,000 equally sized, randomly selected subgroups of participants (gray band = 95% confidence threshold from bootstrap resamples).

Please cite this article in press as: Pines et al., Development of top-down cortical propagations in youth, Neuron (2023), https://doi.org/10.1016/j.neuron.2023.01.014

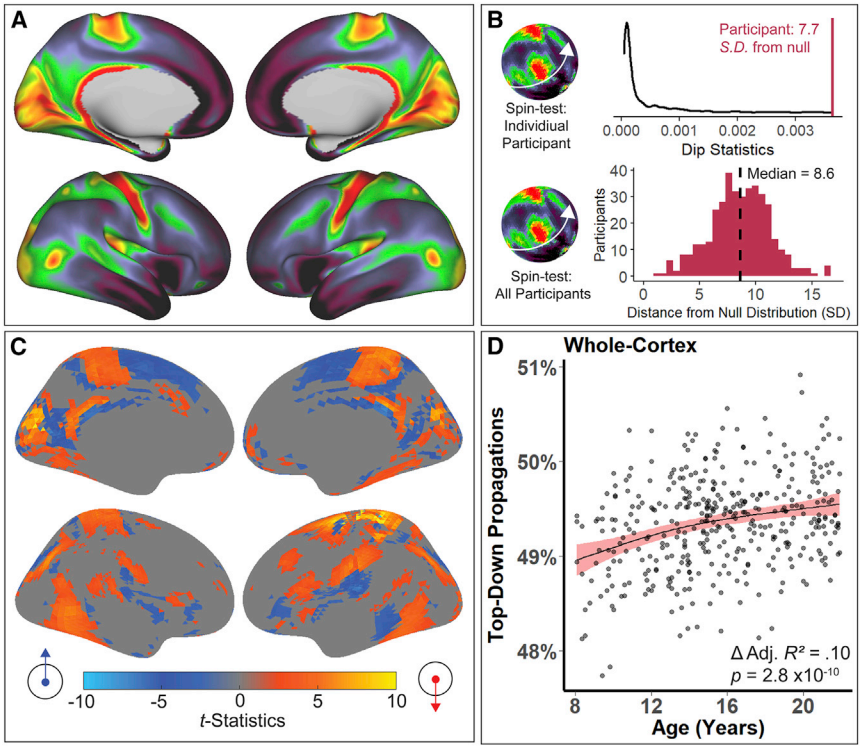

Figure 8. Defining the cortical hierarchy using a measure of intracortical myelin content yields convergent results

(A) Map of the structural hierarchy defined by cortical myelin content.

(B) Bottom-up and top-down propagation directions are also prominent across the structural hierarchy (∇SH), again forming a bimodal distribution for each participant (quantified with dip statistics). Dip statistics obtained for each participant were far greater than those obtained from a spatial null distribution obtained by spinning the myelin map (median SD of observed dip statistic from null distribution = 8.6).

(C) The proportion of bottom-up versus top-down propagations was systematically shifted when rest was compared with a cognitively demanding task and the structural hierarchy was used as the reference ($p_{fdr} < 0.05$).

(D) The prevalence of top-down propagations increased with age when using cortical myelin content to define a structural hierarchy (Δ Adjusted $R^2 = 0.10$, $p = 2.8 \times 10^{-10}$).

remained significant while covarying for default-mode network segregation (Δ Adjusted $R^2 = 0.14$, $p = 1.2 \times 10^{-14}$) and was greater in magnitude than the association between age and default-mode network segregation itself (Δ Adjusted $R^2 = 0.05$, $p = 3.1 \times 10^{-5}$; Figure S6). Next, we sought to verify that our findings were not attributable to developmental differences in the spatial localization of the principal gradient of functional connectivity. Accordingly, we derived principal gradients of functional connectivity for each age tertile of our sample and re-calculated angular distances for each participant relative to the principal gradient for their respective tertile (Figure S7). Dip statistics derived from tertile-specific connectivity gradients were highly similar to those derived from the original group-level map ($r = 0.87$, $p < 2.2 \times 10^{-16}$), and the association between top-down propagations and age remained significant when using tertile-specific functional hierarchies ($p = 9.5 \times 10^{-4}$). Finally, to verify that age effects were not attributable to scanning-site differences, we harmonized fMRI data across sites using ComBat and repeated our main developmental analyses. Developmental effects remained prominent when accounting for site differences with ComBat (Δ Adjusted $R^2 = 0.12$, $p = 2.0 \times 10^{-12}$, Figure S8). Together, these analyses confirmed that our findings were not attributable to previously documented properties of functional neurodevelopment or scanner differences.

DISCUSSION

We capitalized on advances in computer vision and a large dataset of youth with high-quality neuroimaging to delineate activity propagations that traverse the cortical hierarchy in individual participants. Notably, we found that top-down propagations increased during the performance of a demanding cognitive task and become more common with age in youth. These results implicate cortical propagations as a mechanism of hierarchical processing and neurodevelopment.

Cortical surface propagations systematically ascend and descend the cortical hierarchy

Here, we describe the presence of bimodal cortical activity propagations in humans, which ascend and descend the cortical hierarchy. Conservative permutation testing emphasized that cortical activity disproportionately traverses up and down the cortical hierarchy far greater than expected by chance. Notably, both bottom-up and top-down propagations were present in all individuals, as evidenced by bimodal distributions of directional activity flow. Hierarchical propagations were robust to a range of analytic parameters (five orders of spatial regularization magnitude) and evident when either a FH or a SH was used as a reference. Importantly, we similarly found hierarchical propagations in every participant in a dataset of densely sampled adults that was acquired using different scanning parameters with different temporal resolutions (TR = 0.8 and 2.2 s). The generalizability and replicability of our results provides strong evidence of the prevalence of bottom-up and top-down propagations of cortical activity.

Decades of study of the BOLD signal and infraslow (0.01–0.1 Hz) cortical fluctuations provide important neurobiological context for the observed propagations. First, existing evidence suggests that BOLD signal fluctuations within a given region reflect infraslow fluctuations in local field potentials,[46–50] and spatially propagating BOLD fluctuations reflect propagating local field potentials.[19,20,50,63] Although infraslow field potentials

Please cite this article in press as: Pines et al., Development of top-down cortical propagations in youth, Neuron (2023), https://doi.org/10.1016/j.neuron.2023.01.014

have long been observed,[64] they have only more recently been accepted as instrumental to functional cortical organization.[65,66] Infraslow fluctuations manifest over larger portions of cortex than faster fluctuations,[67–70] and recent studies provide multimodal evidence that infraslow activity can entrain synchronization, spiking dynamics, and physiological arousal across the brain.[19,20,71–74] Although infraslow entrainment has been repeatedly demonstrated for gamma-oscillations,[19,20,47,48,68,71] we note that oscillations in other frequency bands bear more complex relationships to infraslow activity.[63,75,76] Nonetheless, spatially distributed facilitation and suppression of gamma-band activity may be one role of infraslow cortical propagations across individuals.

A central finding of this study is that the directionality of slow cortical propagations is systematically hierarchical. Our findings cohere with accumulating evidence from intracranial recordings that spatial directionality is a key feature of perception and task execution in other mammals[30–32,39,40,77] as well as reports of bimodal propagation directionality within circumscribed regions.[32,36] Further, recent human neuroimaging studies suggest that macroscale structural brain networks are optimized to support neurotransmission in hierarchical directions.[78,79] Our results cohere with this literature and provide what is to our knowledge the first functional evidence of pervasive bottom-up and top-down propagations in individual humans. Our directional analyses suggest that the FH captured by the principal gradient provides a potentially unifying account of infraslow propagation directionality across all cortical regions in humans. Although our results extensively demonstrate the presence of hierarchical propagations, our insights into the functional role of these propagations are preliminary. These initial results do suggest that hierarchical cortical propagations are involved in hierarchical processing, but the full suite of neurocognitive functions endowed by hierarchically structured propagations is likely to be complex. However, several existing experimental and theoretical accounts of complex spatiotemporal dynamics in cortical propagations provide intriguing evidence regarding why spatial directionality might be a key feature in cortical processing.

Studies focused on sensorimotor regions suggest that the spatial directionality of activity may interact with topographic representations in the cortex. During bottom-up visual processing, propagation directionality has been shown to underlie coordinated inter-regional stimulus encoding through distributed retinotopic propagations.[37,80] In this context, the spatiotemporal trajectory of activity propagations across retinotopic mappings allows for continuous and synchronized activation of spatially distributed but retinotopically equivalent areas. Initial evidence suggests that an analogous pattern of structured activity propagations along topographically organized sensorimotor regions may underlie aspects of somatosensation and coordination of proximal-to-distal limb movements.[81–83] Given the prominence of topographical representations across the cortical sheet,[84–87] the observed spatiotemporal propagations may regularly interact with spatially embedded topographical representations. However, the extent to which topographically-aligned propagations exist in higher-order cortices remains unknown.[88,89]

Although prior investigation of propagation directionality in higher-order cortices has been limited, the computational principles bestowed by cortical waves can provide insight into their roles throughout the cortex.[38] First, as in visual cortex, the spatiotemporally distributed nature of propagations may facilitate the coordination and integration of information over large regions of the brain.[33,41,77,80] Second, in contrast to older views endorsing neuron-specific information selectivity, information representation via distributed activity over time and space can be efficiently encoded,[90,91] can confer increased representational stability,[37,74] and can better account for empirical observations of trial-to-trial variability in neuronal responses.[37,74,90,92] Finally, if cortical propagations can encode sensory information,[81,93] then local modulation of these propagations may serve to process sensory information.[94] In studies of wave dynamics, the spatial and temporal history of a propagation can be recovered from ''ripples'' in the propagation medium at subsequent time points: this is true even in dissipative and chaotic conditions.[38,95] For waves traversing up or down a cortical hierarchy, this suggests that local modulations to that wave would naturally ingrain modulation history into the wave. Consequently, where in the hierarchy the modulation came from, as well as when the modulation was made, could potentially be recovered from the form of the wave after modulation. As cortical hierarchies may be evolutionarily selected for precisely because they allow for integrating diverse signal modulations throughout the hierarchy,[10] such functionality would be invaluable for information transfer and hierarchical control. Indeed, recent evidence suggests that higher-order cortices act in a top-down fashion on lower-order cortices by priming them for rapid neurotransmission via modulation of ongoing activity fluctuations.[94,96] Relatedly, we observed systematic modulation of cortical propagations in response to task demands, potentially consistent with top-down processing. Together, our results suggest that bottom-up and top-down cortical activity propagation patterns may be important for hierarchical cortical information processing.

The development of top-down propagations

The prevalence of top-down propagations increased with age across the entire cortex as well as focally in several canonical processing streams. Specifically, we observed evidence for the involvement of the dorsal stream, the ventral stream, and premotor pathways. Prior work in animals has revealed top-down propagations in canonical processing streams,[40,77,97,98] suggesting that developmental increases in top-down propagations may to some degree occur where top-down propagations are common. However, the global age effect was nearly as strong as that of any single location on the cortex. This suggests that maturation may entail widespread increases in top-down propagations in addition to enhanced top-down propagations in specific canonical processing streams. In light of recent work highlighting individual differences in the localization of higher-order processes,[12,99–101] the spatially diffuse increases in top-down propagations we observed with age also suggest that top-down maturation may occur heterogeneously across the cortex for different individuals. Irrespective of spatial localization, our developmental results identify top-down propagations as a potential macroscale functional mechanism underlying the maturation of top-down cognition.

Please cite this article in press as: Pines et al., Development of top-down cortical propagations in youth, Neuron (2023), https://doi.org/10.1016/j.neuron.2023.01.014

At the synaptic level, top-down cortical propagations may be facilitated by cholinergic neurotransmission. Although other neurotransmitters are likely to play important roles,[102,103] convergent evidence from cell-staining,[104–107] experimental loss-of-function studies,[106,108–111] and group-average fMRI activation patterns[19,27,112] has consistently implicated cholinergic neurotransmitter systems broadly as causal in top-down cortical activity.[113–117] Further, changes in cholinergic tone are sufficient to modulate cortical propagation dynamics,[118] and a recent report implicates cholinergic neurotransmission in the maturation of top-down processing in mice.[111]

One means by which cholinergic maturation may manifest at larger scales is by biasing allocation of attention. In hierarchical processing, cholinergic projections are able to enhance selective attention toward goal-directed behavior specifically because they induce top-down biasing of local sensory neurons.[98,116,119–121] In instances where multiple salient stimuli compete for attention—such as cluttered visual scenes—top-down activity can bias conflict resolution within sensory cortices away from immediately salient stimuli in support of high-level goal pursuit.[97,98,116,121–124] Notably, the gradual enhancement of proactive attention to long-term goals over reactivity to immediately salient stimuli is a critical feature of neurodevelopment.[125,126] Here, we observed increases in top-down propagations during a cognitive task requiring attentional control to facilitate withholding (no go condition) over salient prepotent responses (go condition). Given that we also observed increases in top-down propagations in the same age range that the development of top-down attention has been ascribed to,[13,122] our description of top-down propagation maturation aligns with the development of top-down attentional control. As such, the maturation of top-down propagations may play an important role in cognitive development by promoting goal-directed attention.

Limitations and future directions

Several limitations should be noted. First, the temporal resolution of fMRI restricted our analyses to infraslow frequencies. As prior studies have reported a wide variety of cross-frequency interactions among hierarchical and infraslow propagations,[19,20,63,73,76,77] future work examining propagation patterns across frequency domains may be able to further disentangle such interactions. Second, the cost function of optical flow is agnostic to the sign of the propagating signal: propagating *decreases* in the BOLD signal are also captured by the resulting vector fields. Because hierarchically propagating infraslow activations and deactivations can facilitate or suppress faster rhythms,[19,20] explicitly delineating activations from deactivations is an important step for future work. Third, respiratory[20,127] and vascular[128,129] processes are known to contribute to BOLD signal propagations at similar frequencies. Further analyses of concurrently acquired physiological data[19,20,130] may serve to disentangle their contributions to observed propagations. Fourth, the motion-related signal artifact is likely to impact activity propagations. Consequently, we erred on the side of being extremely stringent in quality assurance—using only low-motion data and statistically controlling for residual motion artifacts in all analyses. Finally, spatial resolution and computational burden hindered the investigation into the role of the subcortex in activity propagations. Evidence across mammals, recording techniques, and experimental methods all suggest that subcortical structures, particularly the nucleus basalis and the thalamus, are extensively involved in top-down cortical propagations.[19,27,104–106,110,112,114,115,131] Furthermore, the role of subcortical structures is likely to be highly complex. For example, in the thalamus, investigations have revealed hierarchical signaling is often bidirectional and context dependent.[132–135] Moving forward, computational advances in the optical flow algorithm and applications to volumetric fMRI with high spatial and temporal resolution data may allow investigators to delineate subcortical contributions to activity propagations.

These limitations notwithstanding, direct quantification of bottom-up and top-down activity on the cortical surface holds substantial promise for several applications. First, the induction of top-down activity remains a central goal of transcranial magnetic stimulation (TMS), but previously few direct measurements of top-down activity have existed.[136] Concurrent TMS and fMRI-based optical flow may allow for more direct quantification of top-down activity induction across stimulation approaches. Relatedly, an explicit goal of neurofeedback protocols is to increase top-down cortical activity.[137] Again, this goal is frustrated by the lack of direct quantification of top-down activity in fMRI measurements. Real-time visualization of cortical propagations may facilitate more direct visualization of top-down activity. Third, top-down deficits have been implicated in the pathology of numerous neuropsychiatric disorders.[16–18] Similarly, although increased top-down activity is a common treatment target, lack of direct quantification of top-down activity has also hindered research into the etiology of and recovery from such conditions. Consequently, understanding if and how top-down deficits in psychopathology are associated with deficits in top-down propagations may allow for an improved brain-based understanding of these disorders. Although top-down cortical propagations may represent only one of many control mechanisms in the brain, the noninvasive quantification of top-down propagations described here may represent a broadly applicable measure for future research.

Conclusion

We demonstrated the presence of activity propagations that preferentially flow up and down the cortical hierarchy. Our observation that top-down propagations increase in response to top-down task demands suggests that such propagations are to some degree state dependent. Finally, the development of top-down propagations with age suggests a potential role for cortical propagations in the development of top-down control in youth. Taken together, our findings suggest that the directionality of propagating cortical activity may be broadly relevant for studies of hierarchical cortical organization and neurodevelopment, with potentially important implications for our understanding of psychopathology and the design of neuromodulatory interventions.

STAR★METHODS

Detailed methods are provided in the online version of this paper and include the following:

- KEY RESOURCES TABLE

SUPPLEMENTAL INFORMATION

Supplemental information can be found online at https://doi.org/10.1016/j.neuron.2023.01.014.

ACKNOWLEDGMENTS

This work was supported by grants from the National Institutes of Health: F31MH123063 (A.P.), K99MH127293 (B.L.), DP2MH119735 (M.S.), R01MH127608 (M.S.), U01MH109985 (L.M.W.), R01MH112847 (T.D.S. and R.T.S.), R01MH123550 (R.T.S.), R01NS060910 (R.T.S.), R01MH123563 (R.T.S.), R01MH096773098A1 (D.A.F.), R01MH115357 (D.A.F.), R37MH125829 (T.D.S.), RF1MH121867 (T.D.S.), R01MH120482 (T.D.S.), R01EB022573 (T.D.S.), RF1MH116920 (T.D.S), R01MH113550 (T.D.S.), the National Institute on Drug Abuse: U01DA041148 (D.A.F.), the National Institute of Biomedical Imaging and Bioengineering: EB022573 (Y.F.), and the National Science Foundation: DGE-1845298 (S.M.W.).

Research reported in this publication was supported by the National Institute of Mental Health of the National Institutes of Health under award number U01MH109589 and by funds provided by the McDonnell Center for Systems Neuroscience at Washington University in St. Louis. The content is solely the responsibility of the authors and does not necessarily represent the official views of the National Institutes of Health.

AUTHOR CONTRIBUTIONS

Conceptualization, A.P.; methodology, A.P.; software, A.P.; validation, A.P., A.S.K., and G.S.; formal analysis, A.P.; investigation, A.P., T.D.S., A.S.K., M.B., M.S., and M.C.; resources, A.P., M.C., S.C., E.F., A.H., A.R.R., T.M.T., D.A.F., and T.D.S.; data curation, A.P., M.C., S.C., E.F., A.H., A.R.R., T.M.T., D.A.F., and T.D.S.; writing – original draft, A.P., A.S.K., T.D.S., and B.L.; writing – review & editing, A.P., A.S.K., B.L., M.B., A.A., D.S.B., M.C., S.C., Y.F., E.F., A.H., A.R.R., M.S., G.S., T.M.T., J.V., S.M.W., R.T.S., L.M.W., D.A.F., and T.D.S.; visualization, A.P.; supervision, T.D.S.

DECLARATION OF INTERESTS

R.T.S. reports consulting income from Octave Biosciences and has received compensation for scientific reviewing from the American Medical Association.

INCLUSION AND DIVERSITY

One or more of the authors of this paper self-identifies as an underrepresented ethnic minority in their field of research or within their geographical location. One or more of the authors of this paper self-identifies as a member of the LGBTQIA+ community. One or more of the authors of this paper received support from a program designed to increase minority representation in their field of research. While citing references scientifically relevant for this work, we also actively worked to promote gender balance in our reference list.

Received: July 3, 2022
Revised: December 8, 2022
Accepted: January 18, 2023
Published: February 17, 2023

REFERENCES

1. Somerville, L.H., Bookheimer, S.Y., Buckner, R.L., Burgess, G.C., Curtiss, S.W., Dapretto, M., Elam, J.S., Gaffrey, M.S., Harms, M.P., Hodge, C., et al. (2018). The Lifespan Human connectome Project in Development: a large-scale study of brain connectivity development in 5–21 year olds. NeuroImage *183*, 456–468.
2. Gordon, E.M., Laumann, T.O., Gilmore, A.W., Newbold, D.J., Greene, D.J., Berg, J.J., Ortega, M., Hoyt-Drazen, C., Gratton, C., Sun, H., et al. (2017). Precision functional mapping of individual human brains. Neuron *95*, 791–807.e7.
3. Harris, J.A., Mihalas, S., Hirokawa, K.E., Whitesell, J.D., Choi, H., Bernard, A., Bohn, P., Caldejon, S., Casal, L., Cho, A., et al. (2019). Hierarchical organization of cortical and thalamic connectivity. Nature *575*, 195–202.
4. Siegle, J.H., Jia, X., Durand, S., Gale, S., Bennett, C., Graddis, N., Heller, G., Ramirez, T.K., Choi, H., Luviano, J.A., et al. (2021). Survey of spiking in the mouse visual system reveals functional hierarchy. Nature *592*, 86–92.
5. Felleman, D.J., and Van Essen, D.C. (1991). Distributed hierarchical processing in the primate cerebral cortex. Cereb. Cortex *1*, 1–47.
6. Mesulam, M.M. (1998). From sensation to cognition. Brain *121*, 1013–1052.
7. Mansouri, F.A., Buckley, M.J., Mahboubi, M., and Tanaka, K. (2015). Behavioral consequences of selective damage to frontal pole and posterior cingulate cortices. Proc. Natl. Acad. Sci. USA *112*, E3940–E3949.
8. Sheth, S.A., Mian, M.K., Patel, S.R., Asaad, W.F., Williams, Z.M., Dougherty, D.D., Bush, G., and Eskandar, E.N. (2012). Human dorsal anterior cingulate cortex neurons mediate ongoing behavioural adaptation. Nature *488*, 218–221.
9. Badre, D., Hoffman, J., Cooney, J.W., and D'esposito, M. (2009). Hierarchical cognitive control deficits following damage to the human frontal lobe. Nat. Neurosci. *12*, 515–522.
10. Nenning, K.H., Xu, T., Schwartz, E., Arroyo, J., Woehrer, A., Franco, A.R., Vogelstein, J.T., Margulies, D.S., Liu, H., Smallwood, J., et al. (2020). Joint embedding: a scalable alignment to compare individuals in a connectivity space. NeuroImage *222*, 117232.
11. Dong, H.M., Margulies, D.S., Zuo, X.N., and Holmes, A.J. (2021). Shifting gradients of macroscale cortical organization mark the transition from childhood to adolescence. Proc. Natl. Acad. Sci. USA *118*. e2024448118.
12. Pines, A.R., Larsen, B., Cui, Z., Sydnor, V.J., Bertolero, M.A., Adebimpe, A., Alexander-Bloch, A.F., Davatzikos, C., Fair, D.A., Gur, R.C., et al. (2022). Dissociable multi-scale patterns of development in personalized brain networks. Nat. Commun. *13*, 2647.
13. Munakata, Y., Snyder, H.R., and Chatham, C.H. (2012). Developing cognitive control: three key transitions. Curr. Dir. Psychol. Sci. *21*, 71–77.
14. Paus, T., Keshavan, M., and Giedd, J.N. (2008). Why do many psychiatric disorders emerge during adolescence? Nat. Rev. Neurosci. *9*, 947–957.
15. Solmi, M., Radua, J., Olivola, M., Croce, E., Soardo, L., Salazar de Pablo, G., Il Shin, J., Kirkbride, J.B., Jones, P., Kim, J.H., et al. (2022). Age at onset of mental disorders worldwide: large-scale meta-analysis of 192 epidemiological studies. Mol. Psychiatry *27*, 281–295.

16. Shanmugan, S., Wolf, D.H., Calkins, M.E., Moore, T.M., Ruparel, K., Hopson, R.D., Vandekar, S.N., Roalf, D.R., Elliott, M.A., Jackson, C., et al. (2016). Common and dissociable mechanisms of executive system dysfunction across psychiatric disorders in youth. Am. J. Psychiatry *173*, 517–526.

17. Klassen, A.F., Miller, A., and Fine, S. (2004). Health-related quality of life in children and adolescents who have a diagnosis of attention-deficit/hyperactivity disorder. Pediatrics *114*, e541–e547.

18. Casey, B.J., Jones, R.M., and Hare, T.A. (2008). The adolescent brain. Ann. N. Y. Acad. Sci. *1124*, 111–126.

19. Gu, Y., Sainburg, L.E., Kuang, S., Han, F., Williams, J.W., Liu, Y., Zhang, N., Zhang, X., Leopold, D.A., and Liu, X. (2021). Brain activity fluctuations propagate as waves traversing the cortical hierarchy. Cereb. Cortex *31*, 3986–4005.

20. Raut, R.V., Snyder, A.Z., Mitra, A., Yellin, D., Fujii, N., Malach, R., and Raichle, M.E. (2021). Global waves synchronize the brain's functional systems with fluctuating arousal. Sci. Adv. *7*, eabf2709.

21. Yousefi, B., and Keilholz, S. (2021). Propagating patterns of intrinsic activity along macroscale gradients coordinate functional connections across the whole brain. NeuroImage *231*, 117827.

22. Margulies, D.S., Ghosh, S.S., Goulas, A., Falkiewicz, M., Huntenburg, J.M., Langs, G., Bezgin, G., Eickhoff, S.B., Castellanos, F.X., Petrides, M., et al. (2016). Situating the default-mode network along a principal gradient of macroscale cortical organization. Proc. Natl. Acad. Sci. USA *113*, 12574–12579.

23. Sepulcre, J., Sabuncu, M.R., Yeo, T.B., Liu, H., and Johnson, K.A. (2012). Stepwise connectivity of the modal cortex reveals the multimodal organization of the human brain. J. Neurosci. *32*, 10649–10661.

24. Sydnor, V.J., Larsen, B., Bassett, D.S., Alexander-Bloch, A., Fair, D.A., Liston, C., Mackey, A.P., Milham, M.P., Pines, A., Roalf, D.R., et al. (2021). Neurodevelopment of the association cortices: patterns, mechanisms, and implications for psychopathology. Neuron *109*, 2820–2846.

25. Buckner, R.L., and Krienen, F.M. (2013). The evolution of distributed association networks in the human brain. Trends Cogn. Sci. *17*, 648–665.

26. Carhart-Harris, R.L., and Friston, K.J. (2010). The default-mode, ego-functions and free-energy: a neurobiological account of Freudian ideas. Brain *133*, 1265–1283.

27. Munn, B.R., Müller, E.J., Wainstein, G., and Shine, J.M. (2021). The ascending arousal system shapes neural dynamics to mediate awareness of cognitive states. Nat. Commun. *12*, 6016.

28. Bassett, D.S., and Sporns, O. (2017). Network neuroscience. Nat. Neurosci. *20*, 353–364.

29. Park, H.J., and Friston, K. (2013). Structural and functional brain networks: from connections to cognition. Science *342*, 1238411.

30. Besserve, M., Lowe, S.C., Logothetis, N.K., Schölkopf, B., and Panzeri, S. (2015). Shifts of gamma phase across primary visual cortical sites reflect dynamic stimulus-modulated information transfer. PLoS Biol. *13*, e1002257.

31. Davis, Z.W., Benigno, G.B., Fletterman, C., Desbordes, T., Steward, C., Sejnowski, T.J., H Reynolds, J., and Muller, L. (2021). Spontaneous traveling waves naturally emerge from horizontal fiber time delays and travel through locally asynchronous-irregular states. Nat. Commun. *12*, 6057.

32. Rubino, D., Robbins, K.A., and Hatsopoulos, N.G. (2006). Propagating waves mediate information transfer in the motor cortex. Nat. Neurosci. *9*, 1549–1557.

33. Sato, T.K., Nauhaus, I., and Carandini, M. (2012). Traveling waves in visual cortex. Neuron *75*, 218–229.

34. González-Burgos, G., Barrionuevo, G., and Lewis, D.A. (2000). Horizontal synaptic connections in monkey prefrontal cortex: an in vitro electrophysiological study. Cereb. Cortex *10*, 82–92.

35. Mohajerani, M.H., Chan, A.W., Mohsenvand, M., LeDue, J., Liu, R., McVea, D.A., Boyd, J.D., Wang, Y.T., Reimers, M., and Murphy, T.H. (2013). Spontaneous cortical activity alternates between motifs defined by regional axonal projections. Nat. Neurosci. *16*, 1426–1435.

36. Bhattacharya, S., Brincat, S.L., Lundqvist, M., and Miller, E.K. (2022). Traveling waves in the prefrontal cortex during working memory. PLoS Comput. Biol. *18*, e1009827.

37. Muller, L., Reynaud, A., Chavane, F., and Destexhe, A. (2014). The stimulus-evoked population response in visual cortex of awake monkey is a propagating wave. Nat. Commun. *5*, 3675.

38. Muller, L., Chavane, F., Reynolds, J., and Sejnowski, T.J. (2018). Cortical travelling waves: mechanisms and computational principles. Nat. Rev. Neurosci. *19*, 255–268.

39. Davis, Z.W., Muller, L., Martinez-Trujillo, J., Sejnowski, T., and Reynolds, J.H. (2020). Spontaneous travelling cortical waves gate perception in behaving primates. Nature *587*, 432–436.

40. Townsend, R.G., Solomon, S.S., Martin, P.R., Solomon, S.G., and Gong, P. (2017). Visual motion discrimination by propagating patterns in primate cerebral cortex. J. Neurosci. *37*, 10074–10084.

41. Zhang, H., Watrous, A.J., Patel, A., and Jacobs, J. (2018). Theta and alpha oscillations are traveling waves in the human neocortex. Neuron *98*, 1269–1281.e4.

42. Kirisits, C., Lang, L.F., and Scherzer, O. (2014). Decomposition of optical flow on the sphere. Int. J. Geomath. *5*, 117–141.

43. Lang, L.F., and Scherzer, O. (2017). Optical flow on evolving sphere-like surfaces. Inverse Probl. Imaging *11*, 305–338.

44. Jonschkowski, R., Stone, A., Barron, J.T., Gordon, A., Konolige, K., and Angelova, A. (2020). What matters in unsupervised optical flow. In Computer Vision – ECCV 2020. ECCV 2020, A. Vedaldi, H. Bischof, T. Brox, and J.M. Frahm, eds. (Springer), pp. 557–572.

45. Shah, S.T.H., and Xuezhi, X. (2021). Traditional and modern strategies for optical flow: an investigation. SN Appl. Sci. *3*, 289.

46. Logothetis, N.K., Pauls, J., Augath, M., Trinath, T., and Oeltermann, A. (2001). Neurophysiological investigation of the basis of the fMRI signal. Nature *412*, 150–157.

47. Pan, W.J., Thompson, G.J., Magnuson, M.E., Jaeger, D., and Keilholz, S. (2013). Infraslow LFP correlates to resting-state fMRI BOLD signals. NeuroImage *74*, 288–297.

48. Nir, Y., Mukamel, R., Dinstein, I., Privman, E., Harel, M., Fisch, L., Gelbard-Sagiv, H., Kipervasser, S., Andelman, F., Neufeld, M.Y., et al. (2008). Interhemispheric correlations of slow spontaneous neuronal fluctuations revealed in human sensory cortex. Nat. Neurosci. *11*, 1100–1108.

49. Nunez-Elizalde, A.O., Krumin, M., Reddy, C.B., Montaldo, G., Urban, A., Harris, K.D., and Carandini, M. (2022). Neural correlates of blood flow measured by ultrasound. Neuron *110*, 1631–1640.e4.

50. Thompson, G.J., Pan, W.J., Magnuson, M.E., Jaeger, D., and Keilholz, S.D. (2014). Quasi-periodic patterns (QPP): large-scale dynamics in resting state fMRI that correlate with local infraslow electrical activity. NeuroImage *84*, 1018–1031.

51. Laumann, T.O., Snyder, A.Z., Mitra, A., Gordon, E.M., Gratton, C., Adeyemo, B., Gilmore, A.W., Nelson, S.M., Berg, J.J., Greene, D.J., et al. (2017). On the stability of BOLD fMRI correlations. Cereb. Cortex *27*, 4719–4732.

52. Burt, J.B., Demirtaş, M., Eckner, W.J., Navejar, N.M., Ji, J.L., Martin, W.J., Bernacchia, A., Anticevic, A., and Murray, J.D. (2018). Hierarchy of transcriptomic specialization across human cortex captured by structural neuroimaging topography. Nat. Neurosci. *21*, 1251–1259.

53. Glasser, M.F., and Van Essen, D.C. (2011). Mapping human cortical areas in vivo based on myelin content as revealed by T1- and T2-weighted MRI. J. Neurosci. *31*, 11597–11616.

54. Glasser, M.F., Coalson, T.S., Harms, M.P., Xu, J., Baum, G.L., Autio, J.A., Auerbach, E.J., Greve, D.N., Yacoub, E., Van Essen, D.C., et al. (2022). Empirical transmit field bias correction of T1w/T2w myelin maps. NeuroImage *258*, 119360.

55. Betzel, R.F., Byrge, L., He, Y., Goñi, J., Zuo, X.N., and Sporns, O. (2014). Changes in structural and functional connectivity among resting-state networks across the human lifespan. NeuroImage *102*, 345–357.

56. Dosenbach, N.U.F., Fair, D.A., Cohen, A.L., Schlaggar, B.L., and Petersen, S.E. (2008). A dual-networks architecture of top-down control. Trends Cogn. Sci. *12*, 99–105.

57. Sherman, L.E., Rudie, J.D., Pfeifer, J.H., Masten, C.L., McNealy, K., and Dapretto, M. (2014). Development of the default mode and central executive networks across early adolescence: a longitudinal study. Dev. Cogn. Neurosci. *10*, 148–159.

58. Grayson, D.S., and Fair, D.A. (2017). Development of large-scale functional networks from birth to adulthood: A guide to the neuroimaging literature. NeuroImage *160*, 15–31.

59. He, W., Sowman, P.F., Brock, J., Etchell, A.C., Stam, C.J., and Hillebrand, A. (2019). Increased segregation of functional networks in developing brains. NeuroImage *200*, 607–620.

60. Owens, M.M., Yuan, D., Hahn, S., Albaugh, M., Allgaier, N., Chaarani, B., Potter, A., and Garavan, H. (2020). Investigation of psychiatric and neuropsychological correlates of default mode network and dorsal attention network anticorrelation in children. Cereb. Cortex *30*, 6083–6096.

61. Wang, C., Hu, Y., Weng, J., Chen, F., and Liu, H. (2020). Modular segregation of task-dependent brain networks contributes to the development of executive function in children. NeuroImage *206*, 116334.

62. Jones, J.S.; CALM Team, and Astle, D.E. (2022). Segregation and integration of the functional connectome in neurodevelopmentally 'at risk' children. Dev. Sci. *25*, e13209.

63. Keilholz, S.D. (2014). The neural basis of time-varying resting-state functional connectivity. Brain Connect. *4*, 769–779.

64. Aladjalova, N.A. (1957). Infra-slow rhythmic oscillations of the steady potential of the cerebral cortex. Nature *179*, 957–959.

65. Palva, S., and Palva, J.M. (2018). Roles of brain criticality and multiscale oscillations in temporal predictions for sensorimotor processing. Trends Neurosci. *41*, 729–743.

66. Mitra, A., and Raichle, M.E. (2016). How networks communicate: propagation patterns in spontaneous brain activity. Philos. Trans. R. Soc. Lond. B Biol. Sci. *371*, 20150546.

67. Liu, Z., Fukunaga, M., de Zwart, J.A., and Duyn, J.H. (2010). Large-scale spontaneous fluctuations and correlations in brain electrical activity observed with magnetoencephalography. NeuroImage *51*, 102–111.

68. Leopold, D.A., Murayama, Y., and Logothetis, N.K. (2003). Very slow activity fluctuations in monkey visual cortex: implications for functional brain imaging. Cereb. Cortex *13*, 422–433.

69. Vanhatalo, S., Palva, J.M., Holmes, M.D., Miller, J.W., Voipio, J., and Kaila, K. (2004). Infraslow oscillations modulate excitability and interictal epileptic activity in the human cortex during sleep. Proc. Natl. Acad. Sci. USA *101*, 5053–5057.

70. Buzsáki, G., Logothetis, N., and Singer, W. (2013). Scaling brain size, keeping timing: evolutionary preservation of brain rhythms. Neuron *80*, 751–764.

71. Orlowska-Feuer, P., Allen, A.E., Brown, T.M., Szkudlarek, H.J., Lucas, R.J., and Storchi, R. (2021). Infra-slow modulation of fast beta/gamma oscillations in the mouse visual system. J. Physiol. *599*, 1631–1650.

72. Stringer, C., Pachitariu, M., Steinmetz, N., Reddy, C.B., Carandini, M., and Harris, K.D. (2019). Spontaneous behaviors drive multidimensional, brainwide activity. Science *364*, 255.

73. Okun, M., Steinmetz, N.A., Lak, A., Dervinis, M., and Harris, K.D. (2019). Distinct structure of cortical population activity on fast and infraslow timescales. Cereb. Cortex *29*, 2196–2210.

74. Engel, T.A., and Steinmetz, N.A. (2019). New perspectives on dimensionality and variability from large-scale cortical dynamics. Curr. Opin. Neurobiol. *58*, 181–190.

75. Palva, J.M., and Palva, S. (2018). Functional integration across oscillation frequencies by cross-frequency phase synchronization. Eur. J. Neurosci. *48*, 2399–2406.

76. Mitra, A., Kraft, A., Wright, P., Acland, B., Snyder, A.Z., Rosenthal, Z., Czerniewski, L., Bauer, A., Snyder, L., Culver, J., et al. (2018). Spontaneous infra-slow brain activity has unique spatiotemporal dynamics and laminar structure. Neuron *98*, 297–305.e6.

77. Aggarwal, A., Brennan, C., Luo, J., Chung, H., Contreras, D., Kelz, M.B., and Proekt, A. (2022). Visual evoked feedforward–feedback traveling waves organize neural activity across the cortical hierarchy in mice. Nat. Commun. *13*, 4754.

78. Vézquez-Rodríguez, B., Liu, Z.Q., Hagmann, P., and Misic, B. (2020). Signal propagation via cortical hierarchies. Netw. Neurosci. *4*, 1072–1090.

79. Parkes, L., Kim, J.Z., Stiso, J., Calkins, M.E., Cieslak, M., Gur, R.E., Gur, R.C., Moore, T.M., Ouellet, M., Roalf, D.R., et al. (2022). Asymmetric signaling across the hierarchy of cytoarchitecture within the human connectome. Sci. Adv. *8*, eadd2185.

80. Zanos, T.P., Mineault, P.J., Nasiotis, K.T., Guitton, D., and Pack, C.C. (2015). A sensorimotor role for traveling waves in primate visual cortex. Neuron *85*, 615–627.

81. Wu, J.-Y., Huang, X., and Zhang, C. (2008). Propagating waves of activity in the neocortex: what they are, what they do. Neuroscientist *14*, 487–502.

82. Takahashi, K., Saleh, M., Penn, R.D., and Hatsopoulos, N.G. (2011). Propagating waves in human motor cortex. Front. Hum. Neurosci. *5*, 40.

83. Riehle, A., Wirtssohn, S., Grün, S., and Brochier, T. (2013). Mapping the spatio-temporal structure of motor cortical LFP and spiking activities during reach-to-grasp movements. Front. Neural Circuits *7*, 48.

84. Harvey, B.M., Klein, B.P., Petridou, N., and Dumoulin, S.O. (2013). Topographic representation of numerosity in the human parietal cortex. Science *341*, 1123–1126.

85. Konen, C.S., Mruczek, R.E.B., Montoya, J.L., and Kastner, S. (2013). Functional organization of human posterior parietal cortex: grasping- and reaching-related activations relative to topographically organized cortex. J. Neurophysiol. *109*, 2897–2908.

86. Peters, A.J., Fabre, J.M.J., Steinmetz, N.A., Harris, K.D., and Carandini, M. (2021). Striatal activity topographically reflects cortical activity. Nature *591*, 420–425.

87. Huber, L., Finn, E.S., Handwerker, D.A., Bönstrup, M., Glen, D.R., Kashyap, S., Ivanov, D., Petridou, N., Marrett, S., Goense, J., et al. (2020). Sub-millimeter fMRI reveals multiple topographical digit representations that form action maps in human motor cortex. NeuroImage *208*, 116463.

88. Hintiryan, H., Foster, N.N., Bowman, I., Bay, M., Song, M.Y., Gou, L., Yamashita, S., Bienkowski, M.S., Zingg, B., Zhu, M., et al. (2016). The mouse cortico-striatal projectome. Nat. Neurosci. *19*, 1100–1114.

89. Patel, G.H., Kaplan, D.M., and Snyder, L.H. (2014). Topographic organization in the brain: searching for general principles. Trends Cogn. Sci. *18*, 351–363.

90. Qi, Y., and Gong, P. (2022). Fractional neural sampling as a theory of spatiotemporal probabilistic computations in neural circuits. Nat. Commun. *13*, 4572.

91. Chen, G., and Gong, P. (2022). A spatiotemporal mechanism of visual attention: superdiffusive motion and theta oscillations of neural population activity patterns. Sci. Adv. *8*, eabl4995.

92. Alexander, D.M., Jurica, P., Trengove, C., Nikolaev, A.R., Gepshtein, S., Zvyagintsev, M., Mathiak, K., Schulze-Bonhage, A., Ruescher, J., Ball, T., and van Leeuwen, C. (2013). Traveling waves and trial averaging: the nature of single-trial and averaged brain responses in large-scale cortical signals. NeuroImage *73*, 95–112.

93. Roland, P.E., Hanazawa, A., Undeman, C., Eriksson, D., Tompa, T., Nakamura, H., Valentiniene, S., and Ahmed, B. (2006). Cortical feedback

depolarization waves: a mechanism of top-down influence on early visual areas. Proc. Natl. Acad. Sci. USA *103*, 12586–12591.

94. Chen, G., and Gong, P. (2019). Computing by modulating spontaneous cortical activity patterns as a mechanism of active visual processing. Nat. Commun. *10*, 4915.
95. Perrard, S., Fort, E., and Couder, Y. (2016). Wave-based Turing machine: time reversal and information erasing. Phys. Rev. Lett. *117*, 094502.
96. Mazzucato, L., La Camera, G., and Fontanini, A. (2019). Expectation-induced modulation of metastable activity underlies faster coding of sensory stimuli. Nat. Neurosci. *22*, 787–796.
97. van Kempen, J., Gieselmann, M.A., Boyd, M., Steinmetz, N.A., Moore, T., Engel, T.A., and Thiele, A. (2021). Top-down coordination of local cortical state during selective attention. Neuron *109*, 894–904.e8.
98. Herrero, J.L., Roberts, M.J., Delicato, L.S., Gieselmann, M.A., Dayan, P., and Thiele, A. (2008). Acetylcholine contributes through muscarinic receptors to attentional modulation in V1. Nature *454*, 1110–1114.
99. Mazziotta, J.C., Woods, R., Iacoboni, M., Sicotte, N., Yaden, K., Tran, M., Bean, C., Kaplan, J., and Toga, A.W.; Members of the International Consortium for Brain Mapping (ICBM) (2009). The myth of the normal, average human brain–the ICBM experience: (1) subject screening and eligibility. NeuroImage *44*, 914–922.
100. Gordon, E.M., Laumann, T.O., Adeyemo, B., and Petersen, S.E. (2017). Individual variability of the system-level organization of the human brain. Cereb. Cortex *27*, 386–399.
101. Cui, Z., Pines, A.R., Larsen, B., Sydnor, V.J., Li, H., Adebimpe, A., Alexander-Bloch, A.F., Bassett, D.S., Bertolero, M., Calkins, M.E., et al. (2022). Linking individual differences in personalized functional network topography to psychopathology in youth. Biol. Psychiatry *92*, 973–983.
102. Aston-Jones, G., and Cohen, J.D. (2005). An integrative theory of locus coeruleus-norepinephrine function: adaptive gain and optimal performance. Annu. Rev. Neurosci. *28*, 403–450.
103. Vijayraghavan, S., Wang, M., Birnbaum, S.G., Williams, G.V., and Arnsten, A.F.T. (2007). Inverted-U dopamine D1 receptor actions on prefrontal neurons engaged in working memory. Nat. Neurosci. *10*, 376–384.
104. Mesulam, M.M., Mufson, E.J., Levey, A.I., and Wainer, B.H. (1983). Cholinergic innervation of cortex by the basal forebrain: cytochemistry and cortical connections of the septal area, diagonal band nuclei, nucleus basalis (substantia innominata), and hypothalamus in the rhesus monkey. J. Comp. Neurol. *214*, 170–197.
105. Levey, A.I., Hallanger, A.E., and Wainer, B.H. (1987). Cholinergic nucleus basalis neurons may influence the cortex via the thalamus. Neurosci. Lett. *74*, 7–13.
106. Buzsaki, G., Bickford, R.G., Ponomareff, G., Thal, L.J., Mandel, R., and Gage, F.H. (1988). Nucleus basalis and thalamic control of neocortical activity in the freely moving rat. J. Neurosci. *8*, 4007–4026.
107. Zhang, S., Xu, M., Chang, W.C., Ma, C., Hoang Do, J.P., Jeong, D., Lei, T., Fan, J.L., and Dan, Y. (2016). Organization of long-range inputs and outputs of frontal cortex for top-down control. Nat. Neurosci. *19*, 1733–1742.
108. Muir, J.L., Everitt, B.J., and Robbins, T.W. (1994). AMPA-induced excitotoxic lesions of the basal forebrain: a significant role for the cortical cholinergic system in attentional function. J. Neurosci. *14*, 2313–2326.
109. Chiba, A.A., Bucci, D.J., Holland, P.C., and Gallagher, M. (1995). Basal forebrain cholinergic lesions disrupt increments but not decrements in conditioned stimulus processing. J. Neurosci. *15*, 7315–7322.
110. Dasilva, M., Brandt, C., Gotthardt, S., Gieselmann, M.A., Distler, C., and Thiele, A. (2019). Cell class-specific modulation of attentional signals by acetylcholine in macaque frontal eye field. Proc. Natl. Acad. Sci. USA *116*, 20180–20189.
111. Falk, E.N., Norman, K.J., Garkun, Y., Demars, M.P., Im, S., Taccheri, G., Short, J., Caro, K., McCraney, S.E., Cho, C., et al. (2021). Nicotinic regulation of local and long-range input balance drives top-down attentional circuit maturation. Sci. Adv. *7*, eabe1527.
112. Liu, X., de Zwart, J.A., Schölvinck, M.L., Chang, C., Ye, F.Q., Leopold, D.A., and Duyn, J.H. (2018). Subcortical evidence for a contribution of arousal to fMRI studies of brain activity. Nat. Commun. *9*, 395.
113. Warburton, D.M., and Rusted, J.M. (1993). Cholinergic control of cognitive resources. Neuropsychobiology *28*, 43–46.
114. Hasselmo, M.E., and McGaughy, J. (2004). High acetylcholine levels set circuit dynamics for attention and encoding and low acetylcholine levels set dynamics for consolidation. In Progress in Brain Research Acetylcholine in the Cerebral Cortex (Elsevier), pp. 207–231.
115. Sarter, M., and Bruno, J.P. (2000). Cortical cholinergic inputs mediating arousal, attentional processing and dreaming: differential afferent regulation of the basal forebrain by telencephalic and brainstem afferents. Neuroscience *95*, 933–952.
116. Schmitz, T.W., and Duncan, J. (2018). Normalization and the cholinergic microcircuit: a unified basis for attention. Trends Cogn. Sci. *22*, 422–437.
117. Lohani, S., Moberly, A.H., Benisty, H., Landa, B., Jing, M., Li, Y., Higley, M.J., and Cardin, J.A. (2022). Spatiotemporally heterogeneous coordination of cholinergic and neocortical activity. Nat. Neurosci. *25*, 1706–1713.
118. Roach, J.P., Ben-Jacob, E., Sander, L.M., and Zochowski, M.R. (2015). Formation and dynamics of waves in a cortical model of cholinergic modulation. PLoS Comput. Biol. *11*, e1004449.
119. Winkowski, D.E., and Knudsen, E.I. (2008). Distinct mechanisms for top-down control of neural gain and sensitivity in the owl optic tectum. Neuron *60*, 698–708.
120. Asadollahi, A., Mysore, S.P., and Knudsen, E.I. (2010). Stimulus-driven competition in a cholinergic midbrain nucleus. Nat. Neurosci. *13*, 889–895.
121. Pinto, L., Goard, M.J., Estandian, D., Xu, M., Kwan, A.C., Lee, S.H., Harrison, T.C., Feng, G., and Dan, Y. (2013). Fast modulation of visual perception by basal forebrain cholinergic neurons. Nat. Neurosci. *16*, 1857–1863.
122. Kim, N.Y., and Kastner, S. (2019). A biased competition theory for the developmental cognitive neuroscience of visuo-spatial attention. Curr. Opin. Psychol. *29*, 219–228. https://doi.org/10.1016/j.copsyc.2019.03.017.
123. Engel, T.A., Steinmetz, N.A., Gieselmann, M.A., Thiele, A., Moore, T., and Boahen, K. (2016). Selective modulation of cortical state during spatial attention. Science *354*, 1140–1144.
124. Shi, Y.L., Steinmetz, N.A., Moore, T., Boahen, K., and Engel, T.A. (2022). Cortical state dynamics and selective attention define the spatial pattern of correlated variability in neocortex. Nat. Commun. *13*, 44.
125. Casey, B.J. (2015). Beyond simple models of self-control to circuit-based accounts of adolescent behavior. Annu. Rev. Psychol. *66*, 295–319.
126. Chatham, C.H., Frank, M.J., and Munakata, Y. (2009). Pupillometric and behavioral markers of a developmental shift in the temporal dynamics of cognitive control. Proc. Natl. Acad. Sci. USA *106*, 5529–5533.
127. Lynch, C.J., Silver, B.M., Dubin, M.J., Martin, A., Voss, H.U., Jones, R.M., and Power, J.D. (2020). Prevalent and sex-biased breathing patterns modify functional connectivity MRI in young adults. Nat. Commun. *11*, 5290.
128. Amemiya, S., Takao, H., Hanaoka, S., and Ohtomo, K. (2016). Global and structured waves of rs-fMRI signal identified as putative propagation of spontaneous neural activity. NeuroImage *133*, 331–340.
129. Aquino, K.M., Schira, M.M., Robinson, P.A., Drysdale, P.M., and Breakspear, M. (2012). Hemodynamic traveling waves in human visual cortex. PLoS Comput. Biol. *8*, e1002435.
130. Matsui, T., Murakami, T., and Ohki, K. (2016). Transient neuronal coactivations embedded in globally propagating waves underlie resting-state functional connectivity. Proc. Natl. Acad. Sci. USA *113*, 6556–6561.
131. Varela, C. (2014). Thalamic neuromodulation and its implications for executive networks. Front. Neural Circuits *8*, 69.

132. Blethyn, K.L., Hughes, S.W., Tóth, T.I., Cope, D.W., and Crunelli, V. (2006). Neuronal basis of the slow (<1 Hz) oscillation in neurons of the nucleus reticularis thalami in vitro. J. Neurosci. *26*, 2474–2486.

133. Mitra, A., Snyder, A.Z., Tagliazucchi, E., Laufs, H., and Raichle, M.E. (2015). Propagated infra-slow intrinsic brain activity reorganizes across wake and slow wave sleep. eLife *4*, e10781.

134. Hughes, S.W., Cope, D.W., Blethyn, K.L., and Crunelli, V. (2002). Cellular mechanisms of the slow (<1 Hz) oscillation in thalamocortical neurons in vitro. Neuron *33*, 947–958.

135. Engel, A.K., Fries, P., and Singer, W. (2001). Dynamic predictions: oscillations and synchrony in top–down processing. Nat. Rev. Neurosci. *2*, 704–716.

136. Banerjee, S., Grover, S., and Sridharan, D. (2019). Unraveling causal mechanisms of top-down and bottom-up visuospatial attention with non-invasive brain stimulation. J. Indian Inst. Sci. *97*, 451–475.

137. Koush, Y., Meskaldji, D.E., Pichon, S., Rey, G., Rieger, S.W., Linden, D.E.J., Van De Ville, D., Vuilleumier, P., and Scharnowski, F. (2017). Learning control over emotion networks through connectivity-based neurofeedback. Cereb. Cortex *27*, 1193–1202.

138. Dale, A.M., Fischl, B., and Sereno, M.I. (1999). Cortical surface-based analysis. I. Segmentation and surface reconstruction. NeuroImage *9*, 179–194.

139. Fischl, B., Sereno, M.I., and Dale, A.M. (1999). Cortical surface-based analysis. II: inflation, flattening, and a surface-based coordinate system. NeuroImage *9*, 195–207.

140. Earl, E., Perrone, A., Feczko, E., and Fair, D. (2020). ABCD-BIDS pipeline. Center for Open Science. https://doi.org/10.17605/OSF.IO/89PYD.

141. Glasser, M.F., Sotiropoulos, S.N., Wilson, J.A., Coalson, T.S., Fischl, B., Andersson, J.L., Xu, J., Jbabdi, S., Webster, M., Polimeni, J.R., et al. (2013). The minimal preprocessing pipelines for the Human Connectome Project. NeuroImage *80*, 105–124.

142. Feczko, E., Conan, G., Marek, S., Tervo-Clemmens, B., Cordova, M., Doyle, O., Earl, E., Perrone, A., Sturgeon, D., Klein, R., et al. (2021). Adolescent brain cognitive development (ABCD) community MRI collection and utilities. Preprint at bioRxiv. https://doi.org/10.1101/2021.07.09.451638.

143. Fair, D.A., Miranda-Dominguez, O., Snyder, A.Z., Perrone, A., Earl, E.A., Van, A.N., Koller, J.M., Feczko, E., Tisdall, M.D., van der Kouwe, A., et al. (2020). Correction of respiratory artifacts in MRI head motion estimates. NeuroImage *208*, 116400.

144. Ou, Y., Akbari, H., Bilello, M., Da, X., and Davatzikos, C. (2014). Comparative evaluation of registration algorithms in different brain databases with varying difficulty: results and insights. IEEE Trans. Med. Imaging *33*, 2039–2065.

145. Horn, B.K.P., and Schunck, B.G. (1981). Determining optical flow. Artif. Intell. *17*, 185–203.

146. Lefèvre, J., and Baillet, S. (2009). Optical flow approaches to the identification of brain dynamics. Hum. Brain Mapp. *30*, 1887–1897.

147. Townsend, R.G., and Gong, P. (2018). Detection and analysis of spatiotemporal patterns in brain activity. PLoS Comput. Biol. *14*, e1006643.

148. Tournier, J.D., Calamante, F., and Connelly, A. (2007). Robust determination of the fibre orientation distribution in diffusion MRI: non-negativity constrained super-resolved spherical deconvolution. NeuroImage *35*, 1459–1472.

149. Christiaens, D., Sunaert, S., Suetens, P., and Maes, F. (2017). Convexity-constrained and nonnegativity-constrained spherical factorization in diffusion-weighted imaging. NeuroImage *146*, 507–517.

150. Cieslak, M., Cook, P.A., He, X., Yeh, F.C., Dhollander, T., Adebimpe, A., Aguirre, G.K., Bassett, D.S., Betzel, R.F., Bourque, J., et al. (2021). QSIPrep: an integrative platform for preprocessing and reconstructing diffusion MRI data. Nat. Methods *18*, 775–778.

151. Eriksson, S., Blomberg, L.G., and Weimer, D.R. (2002). Comparing a spherical harmonic model of the global electric field distribution with Astrid-2 observations. J. Geophys. Res. Space Phys. *107* SMP 27-1–SMP 27-12.

152. Klose, A.D., and Larsen, E.W. (2006). Light transport in biological tissue based on the simplified spherical harmonics equations. J. Comput. Phys. *220*, 441–470.

153. Shen, L., Farid, H., and McPeek, M.A. (2009). Modeling three-dimensional morphological structures using spherical harmonics. Evolution *63*, 1003–1016.

154. Tian, Y., Margulies, D.S., Breakspear, M., and Zalesky, A. (2020). Topographic organization of the human subcortex unveiled with functional connectivity gradients. Nat. Neurosci. *23*, 1421–1432.

155. Alexander-Bloch, A.F., Shou, H., Liu, S., Satterthwaite, T.D., Glahn, D.C., Shinohara, R.T., Vandekar, S.N., and Raznahan, A. (2018). On testing for spatial correspondence between maps of human brain structure and function. NeuroImage *178*, 540–551.

156. Hastie, T.J., and Tibshirani, R.J. (1990). Generalized Additive Models (CRC Press).

157. Wood, S.N. (2004). Stable and efficient multiple smoothing parameter estimation for generalized additive models. J. Am. Stat. Assoc. *99*, 673–686.

158. Wood, S.N. (2011). Fast stable restricted maximum likelihood and marginal likelihood estimation of semiparametric generalized linear models. J. R. Stat. Soc. B *73*, 3–36.

159. Wood, S.N. (2013). On p-values for smooth components of an extended generalized additive model. Biometrika *100*, 221–228.

160. Johnson, W.E., Li, C., and Rabinovic, A. (2007). Adjusting batch effects in microarray expression data using empirical Bayes methods. Biostatistics *8*, 118–127.

161. Fortin, J.P., Cullen, N., Sheline, Y.I., Taylor, W.D., Aselcioglu, I., Cook, P.A., Adams, P., Cooper, C., Fava, M., McGrath, P.J., et al. (2018). Harmonization of cortical thickness measurements across scanners and sites. NeuroImage *167*, 104–120.

Please cite this article in press as: Pines et al., Development of top-down cortical propagations in youth, Neuron (2023), https://doi.org/10.1016/j.neuron.2023.01.014

STAR★METHODS

KEY RESOURCES TABLE

REAGENT or RESOURCE	SOURCE	IDENTIFIER
Deposited data		
The Lifespan Human Connectome Project Development (HCP-D)	Somerville et al.[1]	https://humanconnectome.org/study/hcp-lifespan-development
The Midnight Scan Club	Gordon et al.[2]	https://openfmri.org/dataset/ds000224/
Software and algorithms		
MATLAB	The MathWorks	Mathworks.com
R	The R Project	r-project.org
Python	Python Software Foundation	Python.org
ABCD-BIDS pipeline	Earl et al.[138]	https://doi.org/10.17605/OSF.IO/89PYD
Spherical Optical Flow	Kirisits et al.[42]	zenodo.org/record/1238901
Freesurfer	Dale et al.[138], Fischl et al.[139]	surfer.nmr.mgh.harvard.edu/
Hierarchical propagation approach	This paper	https://doi.org/10.5281/zenodo.7542444

RESOURCE AVAILABILITY

Lead contact

Further information and requests for resources should be directed to and will be fulfilled by the lead contact, Theodore D. Satterthwaite (satterth@pennmedicine.upenn.edu).

Materials availability

This study did not generate new unique reagents.

Data and code availability

HCP-D and the Midnight Scan Club are publicly available datasets.[1,2] All analysis code and a step-by-step replication guide is available on Github: https://github.com/PennLINC/DevProps.

METHOD DETAILS

Developmental dataset: HCP-D

To evaluate the maturation of cortical propagations, we used high-quality resting-state and task-fMRI data from the Human Connectome Project-Development 2.0 Release (HCP-D, n = 652, mean age = 14.4, SD = 4.1 years). Participants were scanned at four sites on 3 Tesla Siemens Prisma platforms. Structural scans consisted of high-resolution MPRAGE T1w images (0.8 mm^3, TR/TI=2,500,1000 ms, TE = 1.8/3.6/5.4/7.2 ms, flip angle = 8°) and a variable-flip-angle turbo-spin-echo T2w sequence (0.8 mm^3, TR/TI=3,200,564 ms, turbo factor = 314). Additionally, each subject underwent 26 minutes of resting-state scans across 4 runs, and 8 minutes of task-fMRI across 2 runs for our task of interest.[1] Multiband acquisitions afforded sub-second temporal resolution for all functional images (2.0 mm^3, TR/TE = 800/37 ms, flip angle = 52°).

Replication dataset: Midnight scan club

We sought to replicate findings of hierarchical activity propagations in the densely-sampled adults of the MSC. Imaging for each subject was performed on a Siemens TRIO 3T MRI scanner over the course of 12 sessions conducted on separate days, each beginning at midnight.[2] Structural MRI was conducted across two separate days and included T1-weighted images (sagittal, 224 slices, 0.8 mm isotropic resolution, TE = 3.74 ms, TR = 2400 ms, TI = 1000 ms, flip angle = 8 degrees) as well as T2-weighted images (sagittal, 224 slices, 0.8 mm isotropic resolution, TE = 479 ms, TR = 3200 ms). In each session, thirty contiguous minutes of resting state fMRI data were collected, in which subjects visually fixated on a white crosshair presented against a black background. All functional imaging was performed using a gradient-echo EPI sequence (4.0 mm^3, TR/TE = 2,200/27 ms, flip angle = 90°).

Please cite this article in press as: Pines et al., Development of top-down cortical propagations in youth, Neuron (2023), https://doi.org/10.1016/j.neuron.2023.01.014

Image processing

Images from both datasets were processed with an updated version of the Human Connectome Project MRI pipeline.[140,141,142] Specifically, all structural images underwent gradient distortion correction, bias field correction, and normalization to a standard template (MNI). Functional images underwent gradient distortion correction, re-alignment, EPI distortion correction, boundary-based registration, and normalization prior to being projected to the cortical surface and smoothed with a 2mm FWHM gaussian kernel. Functional images were then demeaned and de-trended. Subsequently, nuisance regressors included mean cifti timeseries signal, mean cerebrospinal fluid signal, mean white matter signal, as well as 3 translation (x,y,z) and 3 rotational (roll, pitch, yaw) motion measurements as well as their respective Volterra expansions (derivative, square, and derivative squared of regressor timeseries). Next, functional images were band-pass filtered between 0.008 and 0.09 Hz with a 2^{nd} order Butterworth filter. Framewise displacement was calculated after accounting for the influence of respiratory signal on framewise image realignment.[143] Noteworthy revisions to the standard HCP pipeline included usage of Advanced Normalization Tools (ANTs) for denoising, bias field correction, and diffeomorphic symmetric image normalization, which was selected due to consistently higher registration performance over previous methods.[144] Prior to image analysis, all functional images were downsampled to *fsaverage4* with connectome workbench for computational feasibility.

HCP-D quality control and inclusion criteria

In order to be included in analyses, participants were required to have at least 600 TRs surviving three quality-control thresholds. First, in HCP-D frames were excluded if head motion exceeded 0.2 mm framewise displacement for that frame. Due to the slower sampling rate of the MSC data (TR = 2.2 seconds vs. 0.8 seconds in HCP-D), we relaxed our framewise displacement threshold to 0.4 mm for MSC rather than the 0.2 mm threshold used for HCP-D. Second, frames were excluded if they contained DVARS values that were > 3 standard deviations above the mean. Third, because we were interested in propagations across TRs rather than patterns within single, low-motion TRs, we excluded otherwise low-motion segments that were interrupted by moderate to high-motion frames. Specifically, if TRs that met the first two criteria were not part of a broader sequence of at least 10 consecutive low-motion TRs, these TRs were discarded. In HCP-D, 388 participants (mean age = 15.6, *SD* = 3.7 years) met the > 600 TR requirement after these quality assurance procedures.

As head motion is a major confound in neurodevelopmental imaging, we assessed associations between age and both the number of imaging volumes surviving quality-control and framewise displacement. As expected, age was positively associated with the number of retained imaging volumes (r = 0.35), and negatively associated with head motion within those remaining volumes (r = −0.36). As a result, we controlled for both the number of volumes retained and framewise displacement of retained volumes in all subsequent analyses.

Optical flow

Optical flow is a computer vision technique used to estimate the motion of signal intensity between successive images,[145] which can be applied to neuroimaging to estimate the motion of activity.[146,147] In the current study, we applied a spherical optical flow algorithm[42,43] to spherical registrations of each hemisphere of each participants' cortical mantle.[138,139] Specifically, we used an implementation of optical flow adapted to efficiently estimate biological data occurring on spherical surfaces by use of spherical harmonics and regularizing functionals.[42] This adaptation of optical flow minimizes the following formula:

$$\|\nabla_S F \cdot u + \partial_t F\|^2_{L^2(S)} + \alpha\|u\|^2_{\mu_n}$$

Where F is cortical BOLD signal represented via spherical harmonics, $\nabla_S F$ is the surface gradient of F upon the sphere, u is the vector field being solved for, t is a point in time, and $\partial_t F$ is the partial derivative of the fit harmonics over time. $L^2(S)$ and $\alpha\|u\|^2_{\mu_n}$ serve as norms, facilitating solvable and tractable flow derivations.

Notably, this operates under a brightness constancy assumption. As in image registration, the assumption is that a transformation function φ exists that can reconcile the spatial displacement between two images. Here, this assumption takes the form of:

$$F(t_n, \varphi(t_n, x)) = F(t_0, x)$$

Where t is a point in time, and x is a point in space on the sphere. In our study, this assumption was approximated through the common practice of global signal regression (applied as part of pre-processing), which ensured that net signal was largely constant throughout the functional time series.

This spherical approach provided two primary advantages. First, spherical projection afforded the use of spherical harmonics. Spherical harmonics are a commonly adopted set of basis functions used to represent spherical data in diffusion-weighted imaging[148–150] and in other computational modeling applications.[151–153] Here, we applied spherical harmonics to analytically represent BOLD signal at each spherically-projected hemisphere at each time point. In turn, this step provided computational efficiency to solve for the vector field u explaining the movement of signal between each pair of time points for each participant. Second, as 2-dimensional "patch" projections of the cortex incur prominent warping and large discontinuities between spatially adjacent cortices, our use of the spherical implementation of optical flow allowed us to analyze propagations continuously across the cortex with reduced spatial deformation.

Please cite this article in press as: Pines et al., Development of top-down cortical propagations in youth, Neuron (2023), https://doi.org/10.1016/j.neuron.2023.01.014

Defining hierarchical ascent and descent

In order to estimate directions of hierarchical ascent and descent, we extracted the gradient vector field (∇) of an established map that defines the principal gradient (PG[22]) of a functional hierarchy (∇FH) across the cortex. This approach is analogous to that taken in Tian et al.,[154] but extracted across the cortical mantle rather than in subcortical volumetric space. The resultant vector field, describing hierarchical ascent at each face on the cortical mesh, was subsequently used as a common set of reference directions for each participant's optical flow data.

Quantification of angular distances

In order to evaluate directional alignment between optical flow vectors and hierarchical vectors, we evaluated their angular similarities in degrees. Our primary metric of interest was the angle (in degrees) between hierarchical vectors and optical flow vectors. To derive these angles, the 3-dimensional cartesian (x,y,z) vectors describing both vector fields were converted to a spherical coordinate system (azimuth, elevation, rho) via *cart2sphvec* in MATLAB. Because the signal travels across the surface of the sphere rather than into or away from the surface, this conversion obviates the third coordinate (rho). Consequently, we retained azimuth and elevation only for each hierarchical and optical flow vector, which describe directionality on a 2-D tangent-plane at each cortical face (see Figure 1C). From this point, the angular distance was computed as the difference in directional orientation in degrees between ∇FH and the directional vectors returned by optical flow, with 0 degrees indicating perfect alignment (bottom-up flow) and 180 degrees indicating the maximum possible difference (top-down flow). By quantifying this angular distance between the observed direction of propagation and ∇FH, we were able to construct a timeseries of directional vectors that quantify top-down and bottom-up propagations at each cortical location, for each individual. In total, this yielded 4.4 billion directional measurements across all participants, locations, and timepoints.

Simulated data

To test whether optical flow could recover cortical propagations with known directionality, we simulated a wave of BOLD signal with a normal distribution over space traversing from the posterior pole to the anterior pole of the cortex. Temporal duration was set to match the ≈ 20 second hierarchical cortical propagations previously noted in group-averaged data.[19–21] To ensure equivalence with real data, we adapted the code made available online by Laumann et al.[51] to match spectral content of our simulated data with that of a random fMRI scan from our sample. To examine whether our approach would approximate ground truth angular distances, we also generated a scalar map of the anterior-posterior coordinate of each vertex. After taking the gradient (∇) of this posterior to anterior map – ∇Posterior-Anterior – we calculated the angular distance between the optical flow vector fields in the simulated data and the ground-truth ∇Posterior-Anterior map. This provided an equivalent approach to quantifying angular distance from the ∇FH, but in a scenario where the ground-truth was known. To test the significance of the resultant alignment between the obtained optical flow vectors and ∇Posterior-Anterior, we employed conservative spatial null permutation tests. Specifically, we rotated ∇Posterior-Anterior around a sphere 1,000 times to generate null directional maps with conserved spatial covariance using the spin test.[155] We then calculated the proportion of optical flow vectors estimated to be within 90 degrees of ∇Posterior-Anterior and within 90 degrees of the 1,000 rotated ∇Posterior-Anterior maps. Next, we evaluated the mean and standard deviation of these null proportions relative to the proportion derived from the true angular distribution, allowing us to quantify the degree to which angular alignment in the posterior-anterior direction exceeded alignment with similar directional maps. A p value was defined by the number of times (out of 1,000 rotations) that a randomly-aligned direction exhibited greater alignment than the posterior-anterior direction. Further information on the spin test is detailed in the section below.

Statistical testing of alignment with the functional hierarchy

In order to test whether hierarchical ascent and descent were both directional modes in the distribution of optical flow vectors, we employed Hartigan's dip test. Specifically, we used the dip statistic to quantify the deviance of angular distributions from a unimodal distribution: a higher dip statistic indicates that a distribution is more likely bimodal (or multimodal) than unimodal. Subsequently, we compared this measure to dip statistics derived from spatial and temporal null models.

For spatial null models, optical flow angular distances were calculated relative to a spatially permuted ∇FH. By rotating or "spinning" the entire ∇FH continuously in space, local spatial properties of the original map are conserved.[155] Consequently, this procedure yields a more realistic and conservative spatial null model than random permutations where the spatial covariance structure is lost. We performed 1,000 permutations, and 1,000 corresponding null dip statistics were obtained for each participant. The original medial wall and the resultant location to which the medial wall was spun was masked out of the angular distributions derived for each permutation. Finally, to extract a metric comparable across participants, we recorded the number of standard deviations between the true observed dip statistic and the mean of the 1,000 permutations.

For temporal null models, optical flow was re-calculated on temporally permuted data. Specifically, the temporal sequence of fMRI volumes surviving QC was shuffled iteratively for each participant. Because fitting optical flow for a pair of frames is computationally expensive, we were limited to 100 temporal permutations per subject. This process yielded 100 sets of optical flow vectors for each participant's shuffled data. These null sets of vectors were then subjected to the same angular distance calculation (relative to ∇FH),

Please cite this article in press as: Pines et al., Development of top-down cortical propagations in youth, Neuron (2023), https://doi.org/10.1016/j.neuron.2023.01.014

and 100 null dip statistics were subsequently obtained from these distributions. As for the spatial permutation testing, we evaluated the true vs. permuted dip statistics in terms of the number of standard deviations each participant's true dip statistic separated from the null distribution.

Evaluation of optical flow parameters

In order to evaluate if the alignment of propagations with the functional hierarchy was contingent upon a specific set of optical flow parameters, we conducted a parameter sweep across spatial regularizations (α). Specifically, we selected 4 alternative values for α spanning 5 orders of magnitude (0.01 for very low regularization, 0.1 for low regularization, 10 for high regularization, 100 for very high regularization). We then re-ran optical flow on each HCP-D participant with these new parameters. Subsequently, we evaluated the angular distance between optical flow vectors derived across these parameters and ∇FH. Next, we re-calculated our spatial null distribution at each new parameterization for each subject (Figure S4). As prior, we calculated the number of standard deviations that each participant's dip statistic separated from the dip statistics from the null distribution of 1,000 permuted ∇FH maps; this was done for each of the four additional spatial regularization parameters.

Analysis of the impact of task demands

To evaluated how hierarchical propagations are modulated by task demands, we used data from Carit task included in HCP-D as it requires top-down cognitive control. The Carit task is a modified Go/No-Go task, where participants are instructed to make repeated button-presses in response to rapid, consistent visual stimuli (i.e., shapes), which are periodically interrupted by the display of a different stimuli. During these interruptions, the participant is instructed to withhold a button press, probing their ability to suppress their button-pressing response. Because fewer scans were allocated to this task within HCP-D, we relaxed the minimum TR requirement to 300 total TRs for task analyses only. As we compared propagations between task and resting conditions on a within-subject basis, only participants who passed both resting-state quality control (600 TRs, $n = 388$) and task QC (300 TRs, $n = 281$) were included for these analyses.

To test our hypotheses regarding shifts in top-down propagation prominence with task, we quantified the proportion of top-down propagations. Directional vectors that were greater than 90 degrees from ∇FH were considered top-down, while directional vectors that were less than 90 degrees were considered bottom-up. When averaged across timepoints, this procedure provided a measure of the prevalence of top-down propagations at each cortical face for each participant.

We next compared the proportion of top-down propagations during rest and under the cognitive control demands of the Carit Task. Specifically, we used a paired t-test to compare the proportion of top-down propagations at each cortical face. This procedure provided a t-statistic quantifying the degree to which faces exhibited more top-down propagations during the task than during rest. Multiple comparisons were controlled by the false-discovery-rate (FDR: $q < 0.05$).

Analysis of developmental effects

Developmental effects were estimated using generalized additive models (GAMs)[156,157] with penalized splines in R (Version 3.6.3) using the *mgcv* package. Non-linearity was penalized to avoid over-fitting, and fitting was optimized with restricted maximum likelihood.[158] Participant sex, in-scanner head motion, and the number of frames passing quality assurance were included as covariates within each GAM. Four basis functions were specified as the maximum flexibility afforded to age splines in all models. To quantify the effect sizes of each age spline, we calculated the change in adjusted R^2 ($\Delta R^2_{adj.}$) between the full model and a nested model that did not include an effect of age. Statistical significance was assessed using analysis of variance (ANOVA) to compare the full and nested models.[159] As above, multiple comparisons were controlled using the false-discovery-rate ($q < 0.05$). Finally, because $\Delta R^2_{adj.}$ describes effect size but not direction (i.e., increasing or decreasing top-down propagations with age) we extracted and applied the sign of the age coefficient from an equivalent linear model, as in prior work.[12]

To quantify developmental differences in the full distributions of angular distances between optical flow vectors and ∇FH, we compared the oldest and youngest tertiles of all participants. Specifically, we reduced each participant's angular distribution to 18 bins, with each bin comprising a 10-degree span from 0-180 degrees from ∇FH. Each bin represents the percentage of optical flow vectors that fell within a 10-degree window of angular distances from ∇FH (0-10 degrees, 10-20 degrees, etc.). Across participants within each tertile split, the average of these percentages represents the average percentage of total propagations each 10-degree bin encompasses for each age tertile. To observe age-dependent differences, we subtracted the resultant value of each bin in the younger tertile from the resultant values in the older tertile. This approach provided a description of the difference in angular distributions between older and younger participants. However, that difference measure does not provide a statistical test of whether the difference is significant. To evaluate the statistical significance of age effects, we performed a bootstrap procedure, where tertile splits were determined randomly. We repeated the difference-of-distributions procedure described above for 1,000 random tertile splits, producing 1,000 random differences of distributions. Finally, we extracted the 95% confidence interval from these 1,000 distribution differences to obtain an estimate of distribution differences that could be expected by chance alone. Observed differences exceeding this confidence interval were interpreted as true group differences, exceeding those expected by selecting two groups of the same size when the age distribution was random.

Please cite this article in press as: Pines et al., Development of top-down cortical propagations in youth, Neuron (2023), https://doi.org/10.1016/j.neuron.2023.01.014

Specificity and sensitivity analyses

We employed a group-level myelin map as an alternative hierarchy to confirm bottom-up and top-down directionality. We used the transmit bias-corrected myelin map derived from HCP-D[54] for a structural hierarchy[52] (SH). We then extracted the gradient of this map (∇SH) to provide another reference map of hierarchical directionality at each point on the cortex. Because myelin tracks inversely with cortical hierarchy, top-down activity was quantified as optical flow vectors that were parallel with ∇SH rather than antiparallel, as for ∇FH. As prior, we first confirmed that cortical activity propagates up and down this hierarchy more than expected by chance with spin-test based spatial permutations. Next, we evaluated whether top-down propagations relative to ∇SH increased during a Go/No-Go task by re-calculating the equivalent paired-sample t-tests across rest and task data. Finally, we evaluated the average proportion of top-down propagations across the cortex for each participant, also using ∇SH as reference directions rather than ∇FH. We then applied the same developmental model to evaluate increases in top-down propagations with age.

We conducted several final analyses to confirm that our results were distinct from prior reported results and not driven by site effect. First, the age associations we report occur over the same age range as developmental functional network segregation.[12,55] In particular, default mode network segregation has been among the most consistently reported aspect of adolescent functional connectivity maturation.[12,55–62] To ensure that hierarchical development of cortical propagations was not explained by hierarchical development of cortico-functional networks that are typically measured using standard measures of functional connectivity, we repeated our analyses while controlling for developmental network segregation. To do so, we constructed a 17-network group-consensus atlas for the participants in our study with spatially regularized non-negative matrix factorization. Next, we calculated network segregation as prior[13]: the mean between-network coupling of a network with all other networks. We included this value as a model covariate in sensitivity analyses. Based on prior work, we identified which of the delineated networks are those most likely to exhibit developmental segregation. Previously, we have detailed that the functional networks undergoing the most dramatic developmental segregation are those lying at the top of the cortical hierarchy,[12] and other publications have similarly suggested that default-mode networks undergo developmental segregation.[55–62] Accordingly, we evaluated each network for its hierarchical position and overlap with canonical functional networks, and selected the single network fulfilling both *a priori* criteria (high in hierarchy and overlapping with the canonical default mode). Segregation of this network (higher-order default-mode) comprised the metric of interest for our first sensitivity analysis. For tertile-specific principal gradients of functional connectivity, we followed the original procedure outlined in Margulies et al.[22] Specifically, average functional connectivity matrices were derived for each tertile, thresholded at the 90th percentile, converted to cosine similarity matrices, and decomposed with diffusion map embedding. The gradient (∇) of the resultant first components from each tertile were calculated for use as tertile-specific functional hierarchy reference directions.

Finally, to ensure that the association between top-down propagations and age were not attributable to site effects, we harmonized top-down propagations across sites with ComBat.[160,161] This provided a site-harmonized measure of the proportion of top-down propagations exhibited by each participant, which we then tested in the same GAM framework.